In This Issue

Text by Mitch Leslie
mitchleslie@comcast.net

Putting Cyclin E in the trash

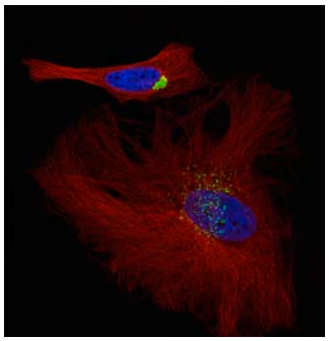

The Golgi apparatus (green) is intact in a control cell (top) but fragmented in a cell lacking RhoBTB3 (bottom).

Lu and Pfeffer uncover a protein that helps remove Cyclin E after it has outlasted its usefulness.

Cyclin E pushes cells from G1 into S phase. But if the protein lingers in cells, they can't progress normally through the rest of the cell cycle. During S phase, the SCF pathway directs phosphorylated Cyclin E to the proteasome for destruction. A second, little-known pathway removes unphosphorylated Cyclin E. This pathway includes the protein Cullin3 (CUL3), which forms part of a ubiquitylating complex. CUL3 partners with proteins in the BTB family, which enable the complex to grab its targets. Lu and Pfeffer tested whether the Golgi-localized BTB protein RhoBTB3 promotes the elimination of Cyclin E.

Cells missing RhoBTB3 arrested in S phase with elevated Cyclin E levels. The Golgi apparatus in these cells also broke up, suggesting that RhoBTB3 helps structure the organelle. RhoBTB3 joined the same ubiquitin-adding complex as CUL3, and it latched onto Cyclin E molecules to spur their ubiquitylation.

The researchers determined that RhoBTB3 functioned properly only if it was located on the Golgi apparatus, yet much of the cell's Cyclin E resides in the nucleus. However, some Cyclin E gathers near the centrosome, which is adjacent to the Golgi apparatus. RhoBTB3 might ensure that the cell disposes of this stockpile of Cyclin E, preventing the centrosome from duplicating more than once.

Lu, A., and S.R. Pfeffer. 2013. *J. Cell Biol.* http://dx.doi.org/10.1083/jcb.201305158.

Polysaccharide's central role in cell division

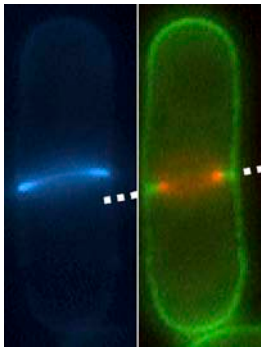

Two views of a cell show that the septum (blue line, left) and the contractile ring (red, right) are tilted in the absence of B-BG.

Muñoz et al. show that a cell wall polysaccharide promotes fungal cell division by helping to center the contractile ring.

During animal cell division, the contractile ring pinches the cell in two, and then the plasma membrane extends to separate the daughter cells. A fungal cell is encased in a cell wall that complicates the division process. As the contractile ring closes and the plasma membrane expands, an extension of the cell wall called the septum stretches across the cell. When this barrier is complete, the central part of the septum deteriorates and the remaining material forms the new end of each daughter cell. The cell wall and septum contain several polysaccharides known as glucans, including branched β(1,3)glucan (B-BG), which is made by the enzyme Bgs4 and helps the cell maintain its shape and integrity. But the role of B-BG during cell division isn't clear.

The contractile ring typically forms in the middle of the cell, but in cells lacking Bgs4 it was often off center and at the wrong angle. Moreover, the ring often slid instead of remaining in place until septum synthesis started. This suggests that B-BG helps situate the contractile ring and hold it in position.

B-BG also helps locate and fortify the septum. The structure normally grows perpendicular to the sides of the cell, but when B-BG was lacking it sometimes formed at an oblique angle or appeared wavy. The septum usually advances across the cell at the same time that the contractile ring closes and the cell membrane extends. But if B-BG was missing, the contractile ring and cell membrane were out of sync with septum growth, suggesting that B-BG helps link all three together so that they progress in unison.

Muñoz, J., et al. 2013. *J. Cell Biol.* http://dx.doi.org/10.1083/jcb.201304132.

Dynamin 2 cuts the cord for newborn lysosomes

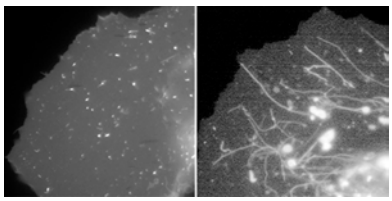

Autolysosomes are small and punctate in a control cell (left), but they swell and grow tubules in the absence of Dynamin 2 (right).

The membrane-snipping protein Dynamin 2 enables cells to burn fat by spurring the formation of new lysosomes, Schulze et al. show.

Many kinds of cells cache lipid droplets that they can consume when nutrients are scarce. One way that cells break down these droplets is through autophagy. A membrane pocket in the cytoplasm encircles a droplet and then merges with a lysosome, forming a structure called an autolysosome that digests the lipids. Autolysosomes sprout buds that detach and mature into fresh lysosomes ready for another delivery of lipids. During endocytosis, the GTPase Dynamin 2 snips free newly formed vesicles. Schulze et al. asked whether the protein performs a similar function during the production of replacement lysosomes.

Knocking down or inhibiting Dynamin 2 suppressed the breakdown of lipid droplets in liver cells, the team found. Lysosomes ballooned to 4–5 times their normal size and sprouted long membranous tubules.

When Schulze et al. dosed liver cells with a Dynamin 2 inhibitor and then removed the compound, some of the tubules that extended from autolysosomes began to fragment. This result suggests that Dynamin 2 helps midwife new lysosomes by cutting them loose from their parental autolysosome. The researchers now want to determine whether Dynamin 2 carries out the same task in other cell types that are reliant on lipid droplets, such as muscle cells and adipocytes.

Schulze, R.J., et al. 2013. *J. Cell Biol.* http://dx.doi.org/10.1083/jcb.201306140.

Extracellular cell wall β(1,3)glucan is required to couple septation to actomyosin ring contraction

Javier Muñoz,[1] Juan Carlos G. Cortés,[1] Matthias Sipiczki,[2] Mariona Ramos,[1] José Angel Clemente-Ramos,[1] M. Belén Moreno,[1] Ivone M. Martins,[1] Pilar Pérez,[1] and Juan Carlos Ribas[1]

[1]Instituto de Biología Funcional y Genómica, Consejo Superior de Investigaciones Científicas/Universidad de Salamanca, 37007 Salamanca, Spain
[2]Department of Genetics, University of Debrecen, 4010 Debrecen, Hungary

Cytokinesis has been extensively studied in different models, but the role of the extracellular cell wall is less understood. Here we studied this process in fission yeast. The essential protein Bgs4 synthesizes the main cell wall β(1,3)glucan. We show that Bgs4-derived β(1,3)glucan is required for correct and stable actomyosin ring positioning in the cell middle, before the start of septum formation and anchorage to the cell wall. Consequently, β(1,3)glucan loss generated ring sliding, oblique positioned rings and septa, misdirected septum synthesis indicative of relaxed rings, and uncoupling between a fast ring and membrane ingression and slow septum synthesis, suggesting that cytokinesis can progress with defective septum pushing and/or ring pulling forces. Moreover, Bgs4-derived β(1,3)glucan is essential for secondary septum formation and correct primary septum completion. Therefore, our results show that extracellular β(1,3)glucan is required for cytokinesis to connect the cell wall with the plasma membrane and for contractile ring function, as proposed for the equivalent extracellular matrix in animal cells.

Introduction

Cytokinesis is a critical process for cell integrity and is very well conserved from animal to fungal cells. All require coordinated contractile actomyosin ring (CAR) closure and plasma membrane (PM) extension. Fungal cytokinesis requires the additional synthesis of a special division wall termed septum, strictly coupled to CAR contraction and PM extension (Pollard, 2010; Balasubramanian et al., 2012). The septum is a three-layered structure of a middle primary septum (PS) flanked by a secondary septum (SS) on each side. The *Schizosaccharomyces pombe* septum grows by simultaneous synthesis of both PS and SS. The last step of cytokinesis is cell separation by controlled cell wall and PS degradation. Correct septum formation and especially cell separation are critical processes for cell integrity and survival (Cabib et al., 2001; Sipiczki, 2007; Cortés et al., 2012).

The fission yeast cell wall contains different essential glucans, but no chitin has been detected (Pérez and Ribas, 2004). Branched β(1,6)glucan is located in the cell wall and SS; minor linear β(1,3)glucan (L-BG) is located mainly in the PS and some in the cell wall; and major branched β(1,3)glucan (B-BG) and α(1,3)glucan are located in the cell wall and both PS and SS (Humbel et al., 2001; Cortés et al., 2007; Cortés et al., 2012). L-BG is a special glucan necessary, but not sufficient, for PS formation that interacts with high affinity with the fluorochrome Calcofluor white (CW) in *S. pombe* (Cortés et al., 2007). B-BG and α(1,3)glucan are essential for cell shape and integrity (Ribas et al., 1991; Hochstenbach et al., 1998; Katayama et al., 1999; Cortés et al., 2005, 2012). α(1,3)glucan is essential for the PS adhesion strength needed to support the internal pressure during cell separation (Cortés et al., 2012). However, the B-BG functions for cell wall and septum structure and integrity remain unknown.

S. pombe contains four essential integral PM glucan synthases (GS) that localize to the CAR, septum, and growing poles. Bgs1 and Ags1 appear simultaneously at the division site before septum synthesis, whereas Bgs4 localizes after septum

Correspondence to Juan Carlos Ribas: ribas@usal.es

Abbreviations used in this paper: B-BG, branched β(1,3)glucan; CAR, contractile actomyosin ring; CW, Calcofluor white; DR, dense ring; GS, glucan synthase; L-BG, linear β(1,3)glucan; MD, matériel dense; MM, minimal medium; MTD, matériel triangulaire dense; OE, old end; PM, plasma membrane; PS, primary septum; SS, secondary septum; TEM, Transmission electron microscopy; WT, wild type.

The Rockefeller University Press $30.00
J. Cell Biol. Vol. 203 No. 2 265–282
www.jcb.org/cgi/doi/10.1083/jcb.201304132

Table 1. **Incorporation of [^{14}C]glucose into cell wall polysaccharides during Bgs4 depletion**

Strain	Thiamine[a]	Incorporation of [^{14}C]glucose[b]			
		Cell wall	α-Glucan[c]	β-Glucan[c]	Galactomannan[c]
	h	%	%	%	%
Control	0 (on)	25.0 ± 2.3	22.2 ± 1.9	62.7 ± 1.4	15.1 ± 0.7
81X-*bgs4*$^+$	6 (off)	23.1 ± 0.7	33.8 ± 4.0	52.4 ± 3.2	13.8 ± 0.8
81X-*bgs4*$^+$	8 (off)	24.0 ± 1.2	40.1 ± 5.1	43.2 ± 6.7	15.8 ± 1.7
81X-*bgs4*$^+$	10 (off)	29.9 ± 0.2	49.2 ± 1.0	35.6 ± 1.5	15.1 ± 0.5

[a]Early log-phase *bgs4*$^+$-repressed cell cultures were grown in MM + 1.2 M sorbitol for 0, 6, 8, and 10 h in the presence of thiamine (*bgs4*$^+$-repressed conditions). [^{14}C]glucose was added 4 h before harvesting.
[b]Percentage of incorporation of [^{14}C]glucose = cpm incorporated per fraction × 100/total cpm incorporated. Values are the means and SDs calculated from three independent experiments.
[c]Values are percentages of the corresponding polysaccharide in the cell wall.

initiation. Bgs1 is responsible for the L-BG and PS synthesis; and Ags1 is responsible for the α(1,3)glucan and SS synthesis and the PS adhesion strength. The function of Bgs3 remains unknown (Cortés et al., 2002, 2005, 2007, 2012; Liu et al., 2002; Martín et al., 2003).

Bgs4 and Ags1 are essential for cell integrity during polarized growth and mainly cytokinesis (Cortés et al., 2005, 2012). Bgs4 is responsible for the cell wall B-BG synthesis and the major β(1,3)GS activity. Bgs4 is also responsible for the resistance to specific β(1,3)GS inhibitors (Ribas et al., 1991; Castro et al., 1995; Cortés et al., 2005; Martins et al., 2011).

In this work, in addition to our findings concerning the essential Bgs4 B-BG functions for the cell wall and septum structure and integrity, we show for the first time that extracellular B-BG is important for CAR positioning in the cell middle. Furthermore, B-BG plays a role in coupling septum synthesis to CAR contraction and PM extension. Our findings reveal important similarities between the function of B-BG in connecting cell wall to CAR and determining intracellular functions of cytokinesis and an analogous role suggested for the ECM (functional equivalent of the cell wall) in animal cells (Xu and Vogel, 2011).

Results

Bgs4 is essential for cell integrity mainly during cytokinesis

To study the essential functions of β(1,3)GS Bgs4, a *bgs4*Δ strain containing integrated *bgs4*$^+$ regulated by the 81X version (highest repression level) of the thiamine-repressible *nmt1*$^+$ promoter, was made (see Materials and methods). The 81X-*bgs4*$^+$ strain showed a uniform repression phenotype of cell lysis. Cell growth arrested after 8 h of *bgs4*$^+$ repression and sorbitol delayed growth arrest to 12 h (Fig. S1 A, arrow). Thus, sorbitol was selected to study stronger *bgs4*$^+$ repression defects in cells that would otherwise be dead. Cell lysis in the presence of sorbitol started at 8 h (Fig. S1, B and D [arrows]), earlier than cell growth arrest was detected, and reached 50% at 12 h. Cell lysis without sorbitol also started earlier than cell growth arrest, at 5–6 h (unpublished data). Coincident with the cell lysis, the increase in cell number also arrested at 8 h (Fig. S1 C, arrow). This discrepancy between absorbance arrest and start of cell lysis was also detected with α(1,3)GS *ags1*$^+$ repression (Cortés et al., 2012). This could be because of additional absorbance of lysed cells, released cytoplasmic material, or changes in cell shape, density, cell wall thickness, or cell wall composition. Most of the lysis occurred at the septum and very little at the poles (Fig. S1 D). In agreement with previous data from *bgs4*$^+$ point mutants (Ribas et al., 1991), the Bgs4-depleted cells showed a considerable decrease in total cell wall β-glucan (56%) and the corresponding compensatory increase in α-glucan (Table 1 and Fig. S1 E).

The Bgs4 amount was analyzed during Bgs4 depletion. Compared with other essential GS, the native expression of Bgs4 is by far the most abundant: 44-fold Bgs1, 9-fold Bgs3, and 6-fold Ags1 (Fig. S1 F). During *bgs4*$^+$ repression, Bgs4 decreased rapidly to 20% at 8 h, when lysis started, and at 12 h it was just 5% of the native level (Fig. S1 G). Therefore, a fivefold Bgs4 reduction is critical for cell wall and septum formation and cell integrity. Also, GFP-Bgs4 localization during repression decreased quickly; at 8 h it was not detected at the poles and at 10 h it was not detected at the septum (Fig. S1 H).

Bgs4 is required for correct PS completion

To know the Bgs4 function in septum formation precisely, the septation defects caused by Bgs4 absence were analyzed. The septation percentage increased after 8 h of *bgs4*$^+$ repression, when cell lysis started, reaching twice the amount of septa at 12 h. This increase was detected only considering live cells. When lysed cells were included (total cells), the septation index was unaffected (Fig. 1 A, left). CW specifically stains the PS (Cortés et al., 2007). CW staining showed a considerable increase in open septa and concomitant decrease in complete septa, generated during the period of lysis induction (Fig. 1 A, right).

To confirm the Bgs4 importance in septum completion, the septa were observed simultaneously by CW staining and GFP-Bgs1 localization. Surprisingly, many CW-stained incomplete septa appeared complete by GFP-Bgs1 (Fig. 1 B, arrowheads). The imbalance between open and complete CW-stained septa was not observed with GFP-Bgs1; instead, the amounts of open and complete septa were unaltered (Fig. 1 C, left). This uncoupling of CW-stained open septa occurred in both growing and complete GFP-Bgs1 septa (Fig. 1 C, right). Thus, Bgs4 absence causes a specific delay in CW-stained PS closure rather than in general cytokinesis completion.

To check if the GFP-Bgs1 advance and closure observed in CW open septa was a process common to all septum components, CW staining and localization of septum membrane Bgs1 and Bgs3 or the CAR components myosin II regulatory chain

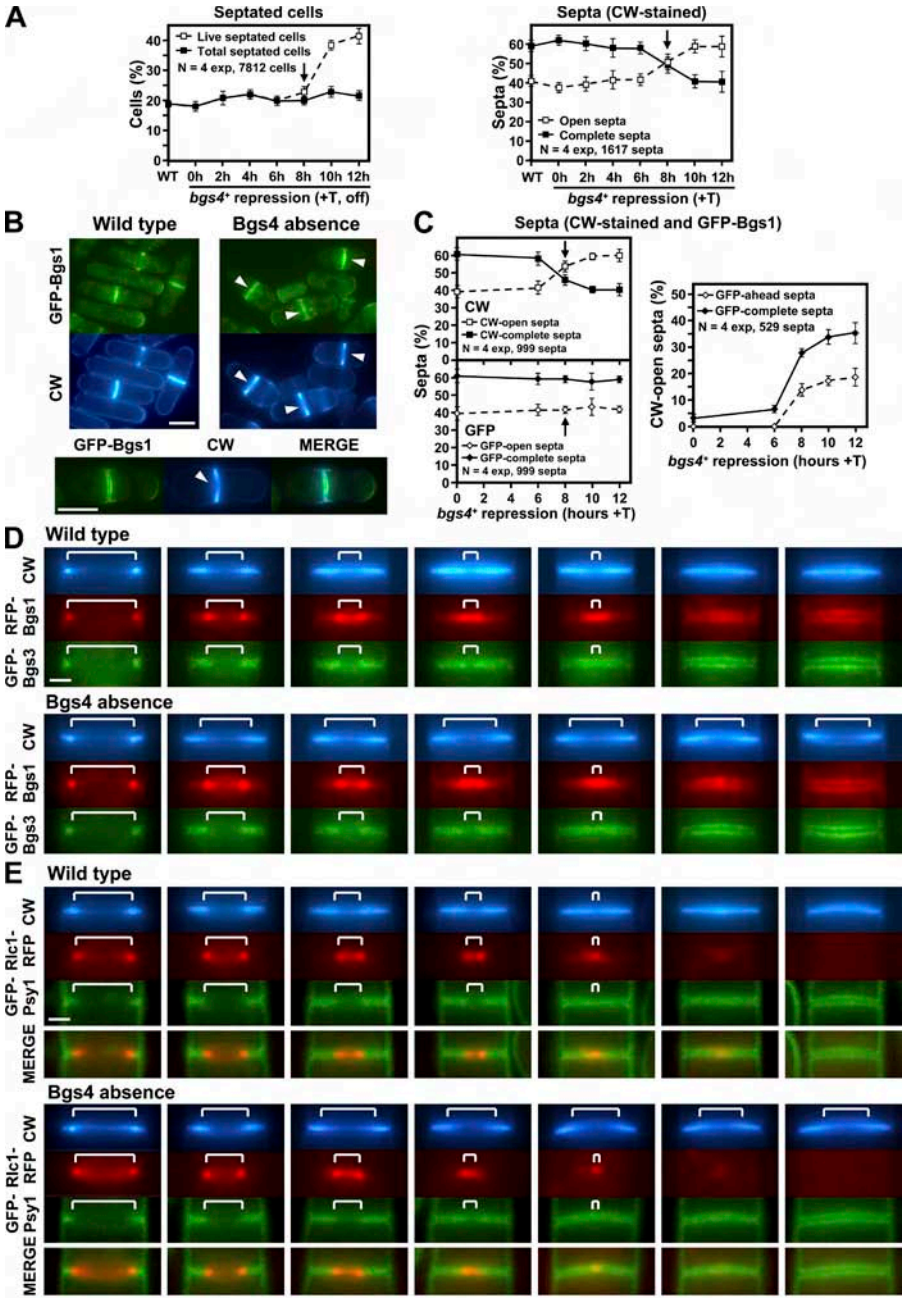

Figure 1. **Bgs4 is required for PS completion but not for general septum closure.** (A) Absence of Bgs4 promotes a septation increase in live but not in total cells (left). Bgs4 absence produces an increase in CW-stained open septa and concomitant decrease in complete septa (right). Arrow shows start of septum defects and cell lysis. Cells were grown in MM with thiamine (+T; repressed) and 1.2 M sorbitol (S). (B) Bgs4 absence causes a defect in CW-stained but not in GFP-Bgs1 septum completion (arrowheads). Cells were grown in MM+S+T for 10 h. (C) Bgs4 absence generates an increase in CW-stained open PS (arrow), not detected in GFP-Bgs1 septa (left). Defective open PS are detected in both advanced (with respect to the CW signal) and complete GFP-Bgs1 septa (right). Cells were grown as in A. Error bars indicate SD. (D) The defect in open PS does not correspond to a general defect in septum synthesis or CAR contraction. Progression (bracket) of WT PS coincides with that of septum membrane (Bgs1, Bgs3, and Psy1) and CAR (Rlc1) proteins but not in the absence of Bgs4, in which the CAR stays attached to the PM, whereas the PS formation is uncoupled and delayed. Cells were grown as in B. The number of experiments and cells or septa analyzed is shown in each case. Bars: (cells) 5 µm; (septum details) 1 µm.

Rlc1 and F-Bar protein Cdc15 (Naqvi et al., 2000; Carnahan and Gould, 2003; Wu et al., 2003), indicative of the growing edge or complete septa, were analyzed simultaneously during *bgs4*$^+$ repression (Fig. 1 D and Fig. S2, A and B). The wild-type (WT) septum showed a coupled progression of CW-stained PS, Bgs1, Bgs3, Rlc1, and Cdc15 (Fig. 1 D and Fig. S2, brackets). In the absence of Bgs4, the CW-stained PS was coincident with CAR and septum membrane proteins only in the early stages of septum formation. In advanced growing and complete septa, the CW-stained PS delayed and uncoupled from Bgs1, Bgs3, Rlc1, or Cdc15 progression (Fig. 1 D and Fig. S2, brackets). A similar CW-stained PS delay was observed with CAR Myo2 and Myo3 and septum Ags1, Rho2-5, Cdc42, Rgf1, and Rgf3 (unpublished data). Simultaneous analysis of CW-stained PS, Rlc1, and the PM syntaxin 1 homologue Psy1 (Maeda et al., 2009) confirmed that the CAR stays attached to the PM when the CW-stained PS is uncoupled (Fig. 1 E, brackets). A similar PS defect was observed in the Bgs4-defective *cwg1-1* and *cwg1-2* mutants (Fig. S5 A, see last section of Results). This defect was not permanent; at longer times the CW-stained PS was completed (see Fig. 4 below). This shows that Bgs4 is specifically required in the last stages of PS formation.

Bgs4 β(1,3)glucan is needed for correct and stable CAR positioning in the cell middle

To investigate other possible Bgs4 functions, the different cytokinesis steps were analyzed after 8 h of *bgs4*$^+$ repression, when cell lysis started, ensuring the presence of mild Bgs4 absence phenotypes and the absence of compensatory mechanisms,

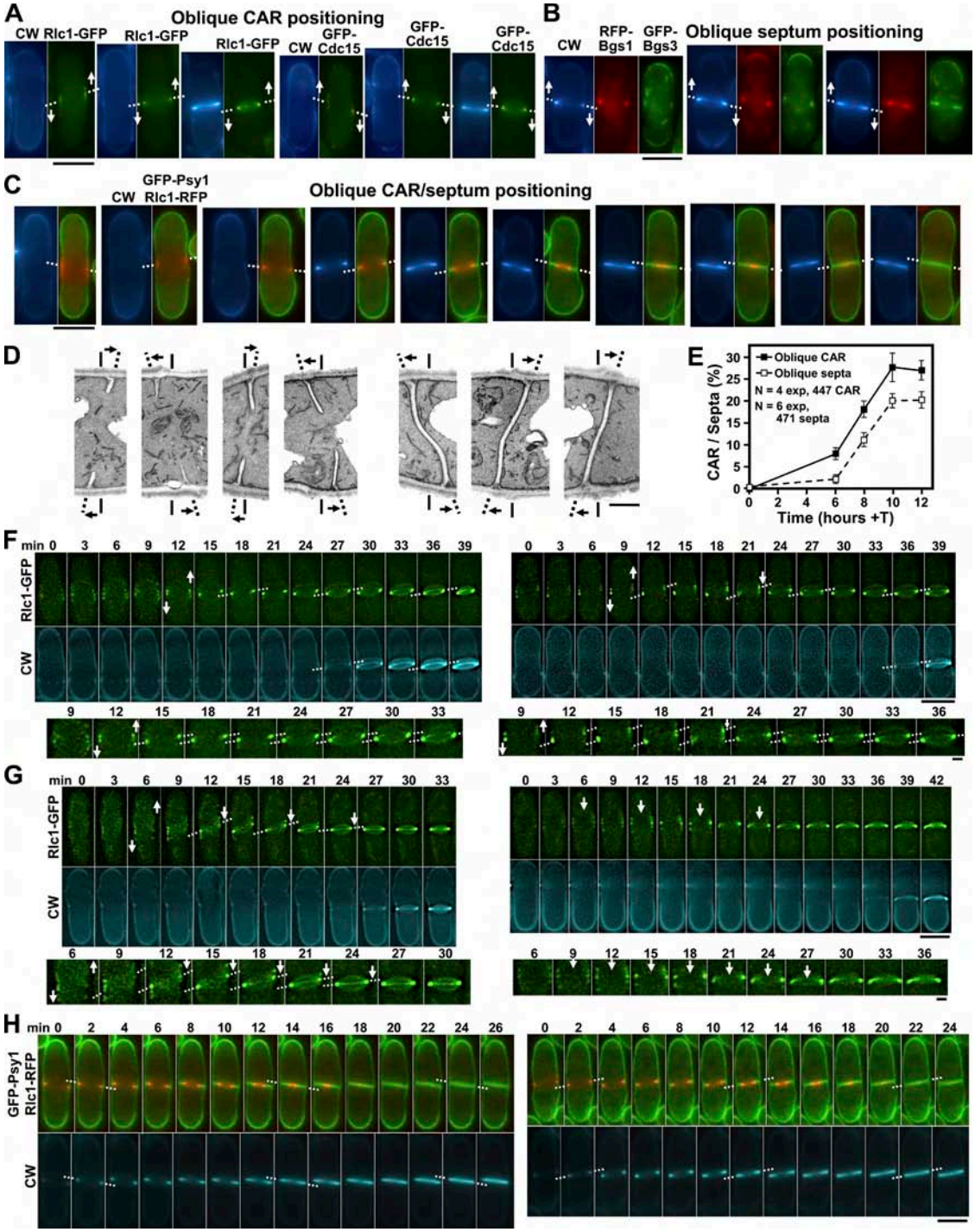

Figure 2. **Bgs4 and its β(1,3)glucan are required for correct and stable CAR positioning in the cell middle.** (A–E) Bgs4 absence generates oblique (dotted line) nodes, CAR (A and C; Rlc1 and Cdc15), and septa (B and C; Bgs1, Bgs3, Psy1, and CW staining). (D) Ultrastructure of oblique (arrow) and misdirected septa. Cells were grown in MM+S+T for 8 h. (E) Percentage of oblique CAR and septa. Error bars indicate SD. (F) Bgs4 absence causes oblique CAR (arrow) in the cell middle that form oblique septa (dotted line). Arrow in dotted line, partial CAR sliding. (G) Bgs4 absence generates defective CAR positioning and sliding in the cell middle until septum synthesis initiation and anchorage to the cell wall. Oblique CAR sliding (arrow) to perpendicular position (left). Perpendicular CAR sliding (right). (H) The defect in Bgs4 function (shown in the *cwg1-2* mutant) causes similar oblique CAR and septa (dotted line). Cells were grown as in Fig. 1 B (F and G) or in YES medium at 25°C and shifted to 37°C for 5–6 h (H) and visualized by time-lapse. Bars: (cells) 5 µm; (septum details) 1 µm.

which were induced at longer times (unpublished data). The absence of Bgs4 generated oblique positioned nodes, CAR, and septa in the cell middle (Fig. 2, A–C, dotted lines). Transmission electron microscopy (TEM) confirmed the formation of oblique septa (Fig. 2 D, arrows). Oblique CAR and septa (Rlc1, Cdc15, Bgs1, Bgs3, and Ags1) were quantified during Bgs4 depletion (Fig. 2 E). Maximal amount of oblique CAR (25%) was higher than that of septa (20%), suggesting that some oblique CAR could slide along the PM and correct their position to perpendicular in the cell middle, before septum synthesis initiation and

anchorage of the septum to the cell wall. The oblique septa (71 oblique septa; $n = 6$) showed a displacement of the septum base with respect to the perpendicular division plane by 0.28 ± 0.2 µm (0.04 ± 0.01 µm in 42 WT cells; $n = 2$) and of the septum center with respect to the cell middle by 0.23 ± 0.1 µm (0.04 ± 0.01 µm in WT). Therefore, the oblique CAR and septa can be positioned in a 0.56-µm middle region, always located in the cell cortex surrounding the nucleus (Rlc1-GFP Hht1-RFP; unpublished data).

To examine the CAR formation and dynamics in the absence of Bgs4 before septum initiation, when CAR position is fixed by the septum anchorage to the cell wall, time-lapses of CAR (Rlc1) and septum (CW staining) formation were performed. Many cells (31%, 11/35) formed a stable oblique CAR and the ensuing oblique septum (Fig. 2 F, dotted lines; and Video 1). In some cases the nodes also condensed in an oblique fashion (Fig. 2, F [right] and G [left]). Interestingly, many oblique CAR (23%, 8/35) slid along the PM to perpendicular position in the cell middle before septation start and some perpendicular CAR also slid along the PM until septum initiation (Fig. 2 G, arrows and dotted lines; and Video 2). The same defect in oblique CAR and septum positioning was observed in the *cwg1-1* and *cwg1-2* mutants (Fig. 2 H, Fig. S3 A, Video 3, and Fig. S5 B, see last section of Results). This shows that Bgs4 is required for proper and stable CAR positioning in the cell middle before septum initiation and anchorage to the cell wall. However, Bgs4 appears in the cell middle after septum initiation (Cortés et al., 2005), indicating that the CAR defects are not caused directly by Bgs4 absence, but by the lack of cell wall B-BG, owing to the Bgs4 defect in previous cycles.

Bgs4 and its β(1,3)glucan are required for correct straight CAR constriction

Absence of Bgs4 led to 20–25% misdirected CAR and septa (Fig. 3, A–D, arrows). A similar defect of misdirected CAR and septa was observed in *cwg1-1* and *cwg1-2* mutants (Fig. S5 C, see last section of Results), being more abundant in *cwg1-1*; therefore, it was selected for time-lapse study (Fig. 3 E, Fig. S3 B, and Video 4). The analysis showed that misdirected ingression could appear and be corrected throughout septum progression, indicating that this defect is independent of the septation stage. In addition, some misdirected edges showed the opposite direction, whereas in others both edges pointed in the same wrong direction (Fig. 3 E and Fig. S3 B, arrows). Detailed CW staining showed wavy PS (Fig. 3 E, bottom right), indicative of multiple minor changes in septum synthesis direction that could not be detected by CAR and PM ingression analysis. TEM confirmed the formation of misdirected septa (Fig. 3 F, arrows). These data suggest the formation of a relaxed CAR unable to provide the tensile force needed for a straight growing septum and a weak flexible septum lacking the rigidity needed for a straight septum structure. In addition, some septa showed simultaneous misdirected progression and defective CW-stained PS, suggesting that ingression can progress with defective PS and CAR forces (Fig. 3 E, Fig. S3 B, and Video 4). However, all misdirected septa were progressively corrected until septum completion, indicating some CAR force.

Bgs4 is required for coupling septum growth to CAR contraction and PM extension

Septation in the absence of Bgs4 was analyzed by TEM. In WT it started with the annular rudiment, a tiny PM invagination of PS, followed by a small septum that already had the three-layered structure of PS flanked by a SS. The septum grew perpendicular to the cell wall, forming a straight rigid structure, and simultaneously the PS drilled into the wall flanked by *matériel triangulaire dense* (MTD; triangular dense material; Fig. 3 F, left). In contrast, Bgs4 absence caused oblique, twisted, and misdirected septa, suggesting weak CAR and PS structures (Fig. 3 F, right, arrows). The SS was absent and the PS only connected to the wall by a thin PS covered by diffuse *matériel dense* (MD; dense material). Interestingly, as the PS progressed, it formed a very thin PS end structure indicative of defective PS synthesis in the last stages of septum formation (Fig. 3 F, right).

Detailed TEM analysis of WT septum showed that PS and PM edges always stayed in close contact (Fig. 3 G, left), indicating that septum growth stays coupled to PM extension and hence to CAR contraction (Fig. 3 H, left). Surprisingly, in the absence of Bgs4, the thinner PS edge (Fig. 3 G, right, arrowheads) appeared clearly detached and delayed from the PM edge, which formed a sharp tip extension with no PS material inside (Fig. 3 G, right, arrows). Similarly, a more advanced septum closure showed a growing PS but complete PM extension (Fig. 4 F), indicating that septum growth was uncoupled and delayed regarding PM extension and CAR contraction (Fig. 3 H, right). This shows that Bgs4 and/or its B-BG play a role in coupling septum synthesis to PM and CAR progression.

The uncoupling of CAR contraction from septum synthesis was analyzed by time-lapse. The start of CAR contraction and septum synthesis ($t = 0$) was located precisely to the time before the first image when a CW-stained PS signal was detected (Fig. 4 A, blue arrowheads; $t = 2$). In WT cells, the CAR coincided with the edge of the growing PS throughout the contraction process, indicating that CAR contraction and septum synthesis are coordinated (Fig. 4 A and Video 5). In the absence of Bgs4, CAR contraction progressed more slowly than in WT, and septum synthesis advanced much more slowly, delayed and uncoupled from CAR contraction (Fig. 4 A, Fig. S4 A, and Video 6). The analysis of 26 WT and 34 Bgs4-depleted time-lapses showed no significant differences in CAR assembly and maturation. However, Bgs4 absence promoted a 4-min increase (121% of WT) in CAR constriction and an 8.5-min increase (144%) in uncoupled septum synthesis (Fig. 4 B).

Kymographs showed that Bgs4 and its B-BG are critical for the early steps of CAR contraction and septum formation. WT kymograph showed uniform and coincident CAR contraction and PS formation (Fig. 4, C and D). The kymographs of Bgs4 absence showed strong defects in initial CAR contraction and PS formation and a clear delay in PS formation during and after CAR contraction (Fig. 4, C and D; and Fig. S4, B and C). The start of CAR contraction was severely compromised during a 6–8-min period, after which contraction proceeded even faster than in WT. The initial slow CAR contraction was coupled to a defective slow and asymmetric PS synthesis start,

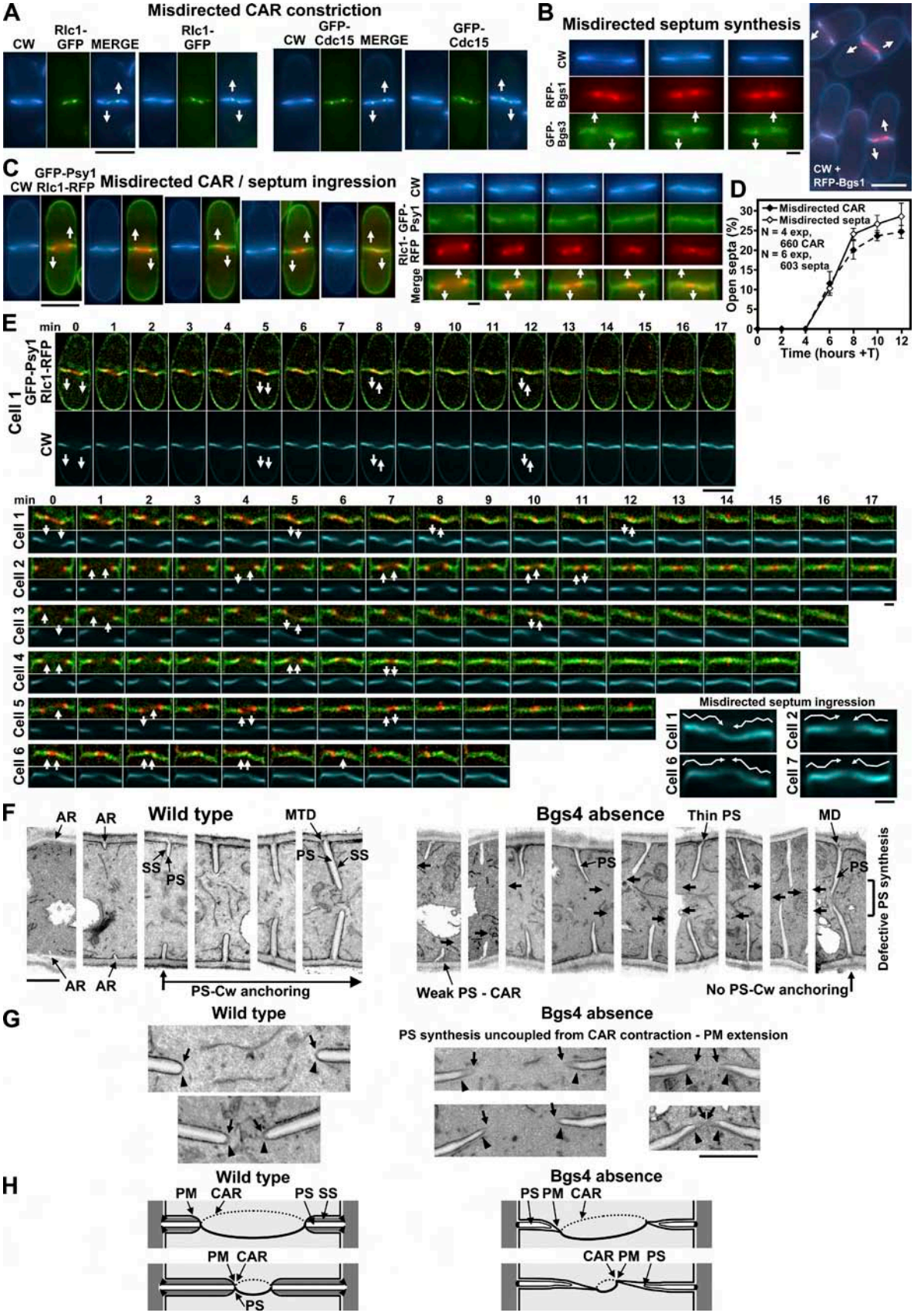

Figure 3. **Bgs4 and its β(1,3)glucan are required for correct straight CAR constriction and for coupling septum synthesis to CAR contraction and PM extension.** (A–D) Bgs4 absence causes misdirected (arrows) CAR (A and C; Rlc1 and Cdc15) and septa (B and C; Bgs1, Bgs3, Psy1, and CW staining). Cells were grown as in Fig. 2 A. (D) Percentage of misdirected CAR and septa. Error bars indicate SD. (E) The defect in Bgs4 function (shown in the *cwg1-1* mutant) produces similar misdirected CAR contraction and septum progression (arrows). During misdirected ingression, the CAR (Rlc1) stays attached to the PM

as observed by the reduced CW staining on one side (Fig. 4, C and E; and Fig. S4 B, white arrows). TEM showed that the asymmetry was coincident with bent or twisted starting septa (Fig. 4 E, black arrows), suggesting that Bgs4 B-BG strengthens the starting septum and that the CAR force is not sufficient to maintain it straight. After this, PS synthesis uncoupled from CAR contraction, starting a delay that increased along septation. The 6-min delay in septum completion (t = 22–28) coincided with TEM observations of growing PS but complete PM extension (Fig. 4 F).

The analysis of WT CAR contraction and PS synthesis rates showed a coincident and constant rate (95 nm/min) throughout the process (Fig. 4 G). However, Bgs4 absence caused an initial slow CAR contraction and septation rate, sevenfold slower than in WT (15 nm/min in both cases). Interestingly, after this defect the CAR contraction rate increased to 127% faster than WT (120 nm/min). The PS synthesis rate also increased, but only to 76% of WT (72 nm/min), confirming the defective and delayed PS synthesis (Fig. 4 G). This suggests that in WT, CAR and PM ingression rates are restricted by the synthesis rate of the attached septum.

Bgs4 β(1,3)glucan confers the rigidity needed for a straight septum

In the absence of Bgs4, the septa presented important morphological and structural defects. Many septa had a curved shape (Fig. 5 A) and defects in PS maturation of CW-stained PS retracted from the cell wall (Fig. 5 B, left, arrowheads and arrows). TEM confirmed the retraction of mature PS, leaving a space filled by new MD (Fig. 5 B, right, arrows). Similar defects were observed in the *cwg1-1* and *cwg1-2* mutants (Fig. S5 D, see last section of Results).

To study the formation mechanism of curved septa, time-lapses of septum formation were performed. WT cells formed a rigid straight septum that, after maturation (11 min), was slowly and symmetrically degraded by its PS to permit sister cell separation (Fig. 5 C, top; and Video 7). In the absence of Bgs4, maturation of some septa extended for a long period (60 min), during which the septa displayed an oscillating curved shape, probably because of changes in internal pressure between sister cells. The lower pressure cell reacted by increasing its internal pressure, pushing the flexible septum and changing its curvature to the opposite cell (Fig. 5 C, middle and bottom, arrow; Fig. S4 D, arrow; and Video 8). In some cases the pressure transmitted by the pushing septum caused pole lysis in the opposite cell (Fig. 5 C, middle; and Fig. S4 D), or the cells equilibrated their internal pressure, returning to a straight septum and causing lysis at the septum region in both cells (Fig. 5 C, bottom). When no lysis occurred, both cells alternated the septum curvature for at least four waving cycles (Fig. 5 D, arrows; and Video 9). This shows that Bgs4 B-BG is necessary to confer the rigidity needed for a straight septum to support the changes in internal pressure between sister cells.

Bgs4 is responsible for the SS formation

Because of the importance of Bgs4 in septum maturation and structure, complete septa were analyzed in detail by TEM. WT complete septa showed a clear transition to thicker septa in a maturation process of a second round of SS synthesis. In addition, the PS appeared well anchored into the cell wall (Fig. 6 A, left). However, in the absence of Bgs4 the septa showed a total absence of SS during septum formation (see Fig. 3 F) and the whole maturation process (Fig. 6 A, right). Although the SS contains different polysaccharides, this shows that Bgs4 B-BG is responsible for the SS formation. Bgs4 is also required for PS completion (see above for Figs. 1 and 4). As a result, the initial complete septa showed a large middle region of defective very thin PS, which during septum maturation was gradually disappearing by addition of new PS material (Fig. 6 A, right).

Detailed TEM study of the PS showed the WT annular rudiments containing a PS formed at the wall surface. During septum growth and maturation, the PS drilled progressively to reach the middle of the cell wall (Fig. 6 B, top, arrows). However, in the absence of Bgs4 the PS was formed with only a very thin and twisted PS base reaching the wall surface. Then, during septum maturation the PS never drilled into the wall but gradually retracted from it, leaving a spaced filled by amorphous MD (Fig. 6 B, bottom, arrows). This shows that Bgs4 is not only required for PS completion but also for the integrity of the PS base and its anchorage into the wall.

Bgs4 is essential for cell integrity at the start of cell separation

The main defect of Bgs4 absence is the lysis and cytoplasm release after septum completion. Lysis occurred in either one or both sister cells, appearing in one single cell earlier than in both cells (Fig. 7, A [arrows] and B). After lysis in one cell, the surviving sister cell initiated a new cell growth cycle, the wall carcass of the dead cell sometimes remaining attached. At later times, the lysis appeared in both cells, probably because of an increase in cell wall weakness (Fig. 7 A). Cell growth is mainly monopolar and therefore most of the new defective wall is located at one pole. After septum synthesis, lysis occurs only on the side of defective cell wall. In the next cell cycle, the defective wall increases, generating after septation the lysis in both cells (Fig. 7 C). Similar cell lysis defects were observed in the *cwg1-1* and *cwg1-2* mutants (Fig. S5 E, see last section of Results).

(Psy1). CW staining shows the details of wavy PS (bottom right, wavy arrow), indicative of relaxed CAR with multiple changes in septum synthesis direction. Cells were grown as in Fig. 2 H and observed by time-lapse. (F) TEM details of rigid and straight WT septum formation with simultaneous PS and SS synthesis from the start (left). Formation in Bgs4 absence of weak twisted and misdirected (arrows) septa with no SS and defects in the last stages of PS synthesis (right). Cells were grown as in A. (G and H) Bgs4 is essential for coupling PS growth to CAR contraction and PM extension. (G) Magnification of septum formation as in F. (H) Model of advanced CAR and PM ingression uncoupled from delayed PS synthesis. A relaxed CAR devoid of tensile force causes misdirected septa. Arrows, CAR and PM edge; arrowheads, PS edge. AR, annular rudiment; Cw, cell wall. Bars: (cells) 5 µm; (septum details) 1 µm.

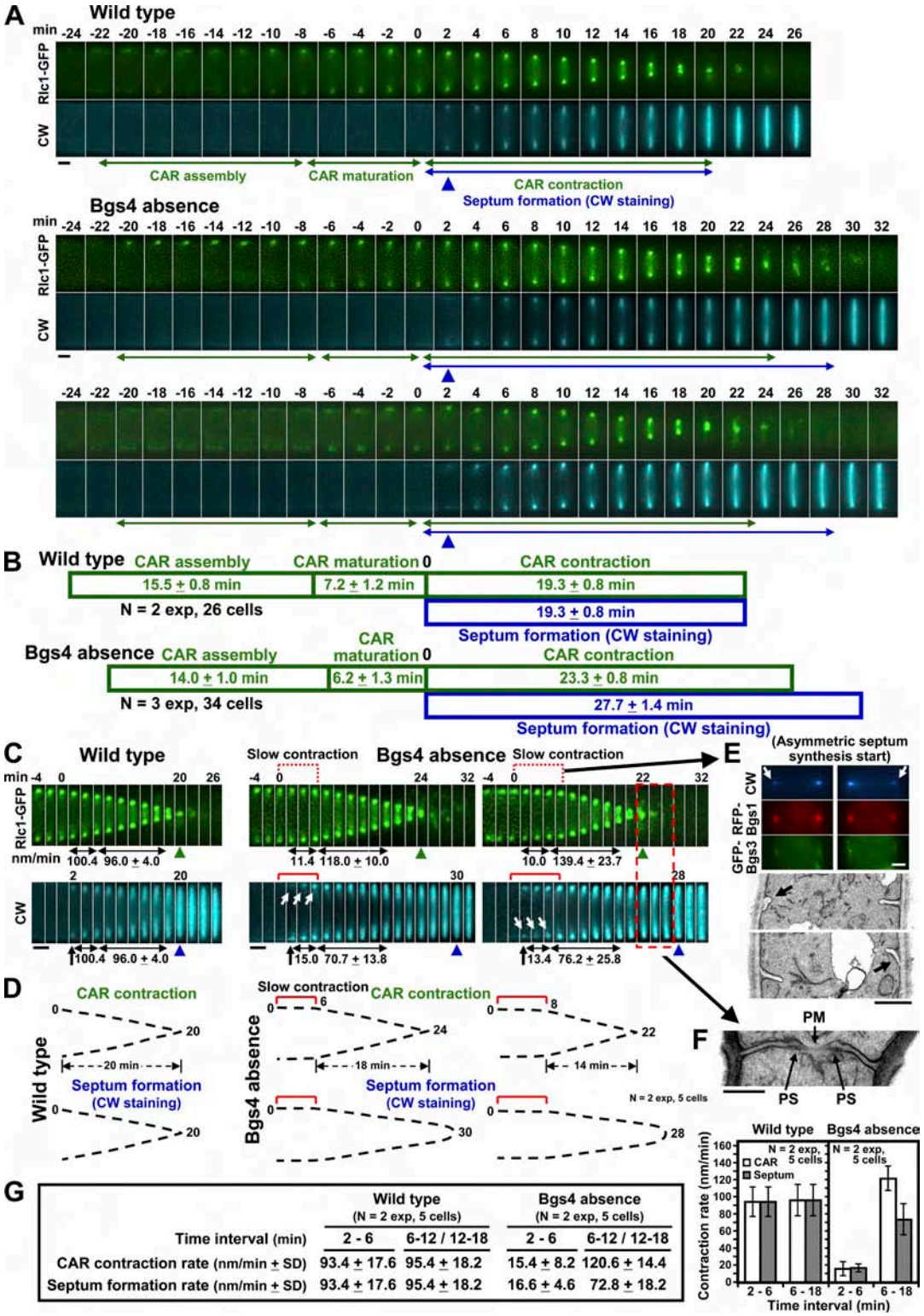

Figure 4. **Bgs4 absence causes a slower septum formation, uncoupled from an altered and faster CAR contraction.** (A and B) WT CAR contraction and PS synthesis are coordinated, whereas Bgs4 absence produces a slower CAR contraction and much slower PS growth. (A) Cells were grown as in Fig. 2 A and imaged by time-lapse. Arrowhead shows first PS signal detected (t = 2), locating in the previous image (t = 0) the simultaneous start of PS synthesis and coupled CAR contraction. (B) The time of CAR assembly, maturation, and contraction and of PS formation was quantified. (C–G) WT CAR contraction and septation are uniform and coincident. In Bgs4 absence, initial CAR contraction and PS formation are strongly impaired (red bracket), but ensuing CAR contraction proceeds faster than in WT and uncoupled from a slower PS formation. (C) Kymographs of the time-lapses of A. (D) Scheme of CAR and PS progression in the kymographs. White arrows show asymmetric septum synthesis start. Arrowhead shows end of CAR contraction (green) and PS formation (blue). Rectangle marks interval (t = 22–26) of growing PS but complete CAR contraction. (E) The slow CAR contraction is coincident with a defective PS synthesis start (arrows). Cells were grown as in A. (F) Detail of defective growing PS uncoupled from complete PM extension. (G) Rates of CAR contraction and PS synthesis (2–6, 6–12, and 12–18 min). Error bars indicate SD. Bars, 1 µm.

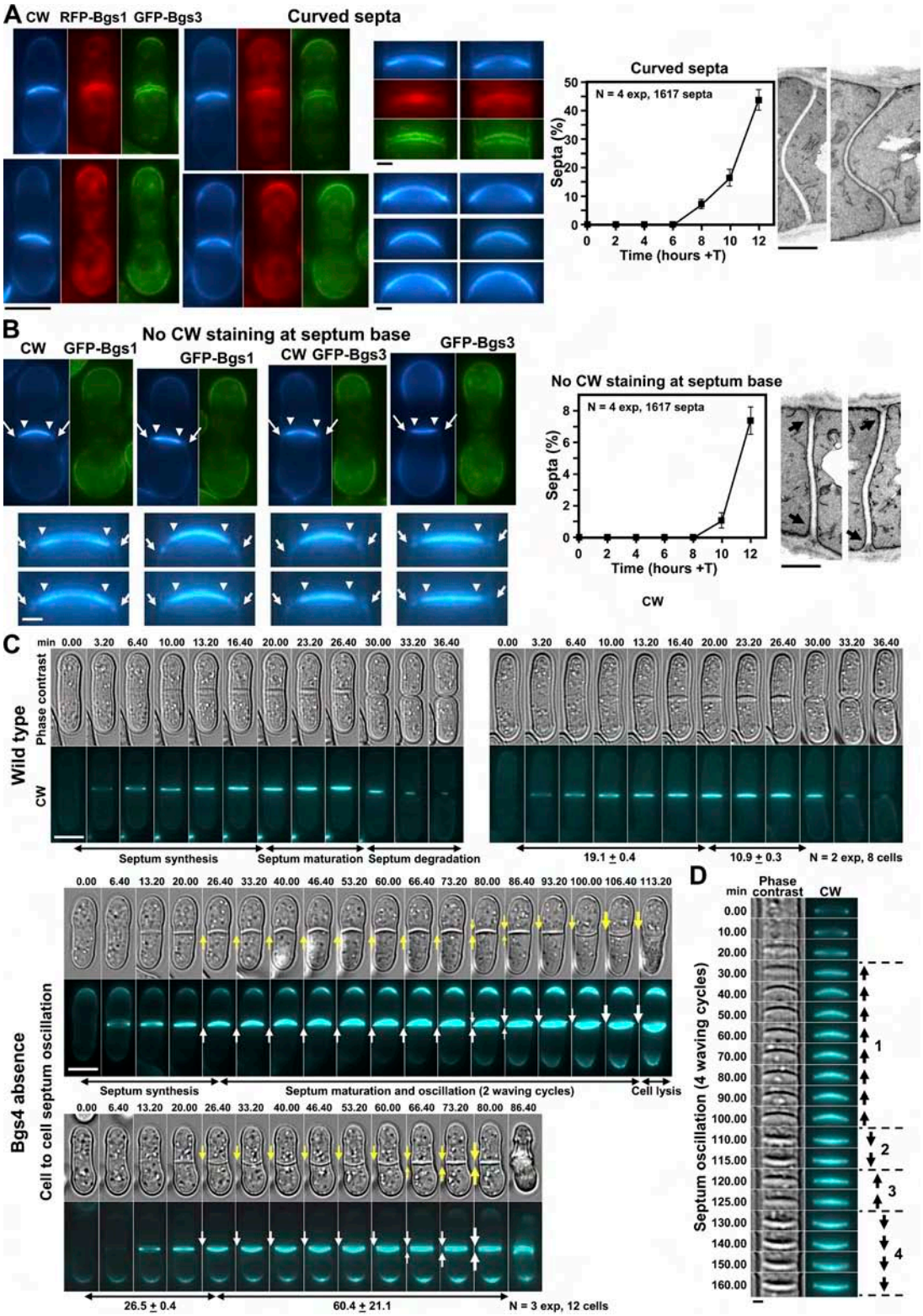

Figure 5. **Bgs4 β(1,3)glucan confers the septum strength needed for a rigid straight septum.** (A and B) Absence of Bgs4 generates curved (A) and defective septa with no CW-stained PS at the septum base (B). Details of PS (arrows) retracted from the cell wall (B, right). Cells were grown as in Fig. 1 B. Arrows, cell wall; arrowheads, CW-stained PS base. Error bars indicate SD. (C and D) Bgs4 absence generates flexible curved septa, oscillating according to the changes in internal pressure between sister cells. Cells were grown in MM+S+T for 9 h and visualized by time-lapse. (C) WT rigid straight septum formation and progressive cell separation (top). Flexible curved septa with two oscillating cycles (arrow), ending with cell lysis in one (middle) or both cells (bottom). (D) Kymograph of a flexible curved septum with four waving cycles (arrow). Bars: (cells) 5 µm; (septum details) 1 µm.

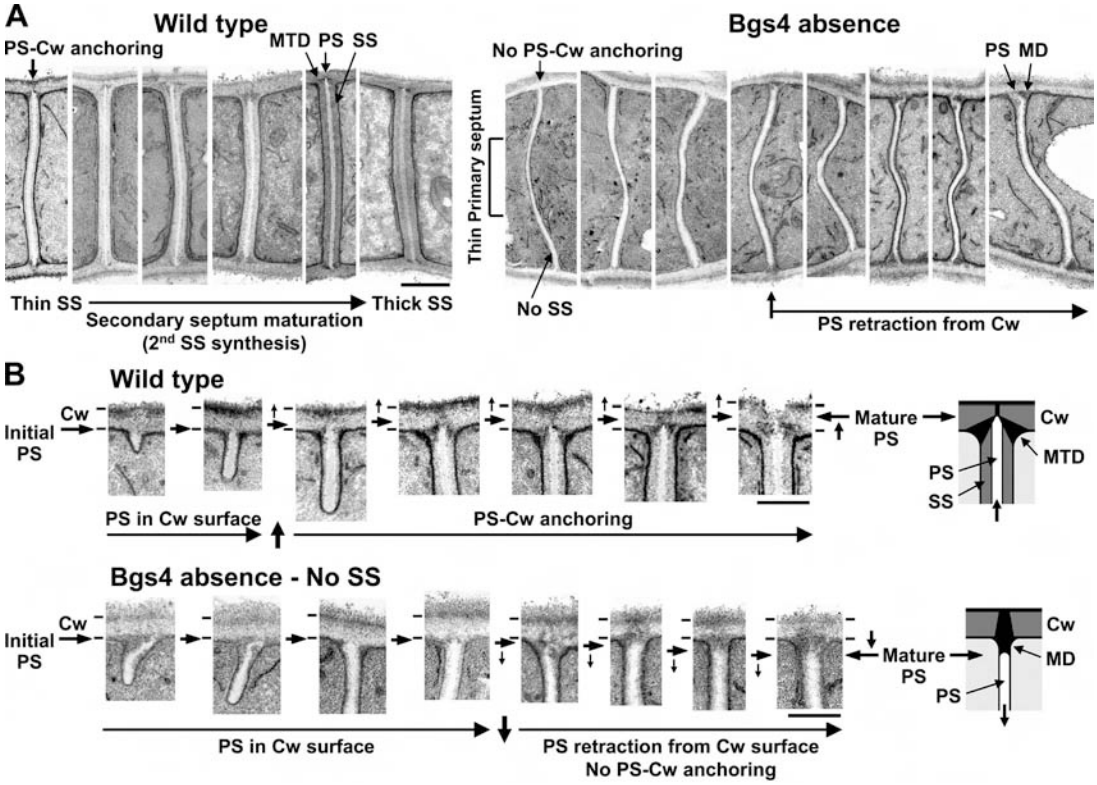

Figure 6. **Bgs4 is responsible for the SS formation and necessary for the integrity of the PS base needed for its anchorage into the cell wall.** (A) TEM details of septum maturation. WT complete septa are straight and increase in thickness by a second round of SS synthesis (left). Bgs4 absence causes the total absence of SS. The complete septa are twisted and the middle region is extremely thin as a result of the defect in PS completion. During maturation, the thin central region is repaired by addition of new PS (right). Cells were grown as in Fig. 2 A. (B) Details of PS anchorage or retraction during septum maturation. WT PS starts in the cell wall (Cw) surface. During septum growth and maturation the PS is progressively anchored into the cell wall (top). In Bgs4 absence, the defective PS progressively retracts from the cell wall, leaving a space filled by MD (bottom). Bars: (A) 1 µm; (B) 0.5 µm.

To know the precise timing of cell lysis, the process was analyzed by time-lapse. After septum completion and maturation, an abrupt cell wall and PM rupture released the cytoplasmic material from either one or both cells (Fig. 7 D, arrow; Fig. S4 E, arrow; and Video 10). No cell separation was detected, indicating that lysis occurred just after septum maturation and before or at the start of cell separation.

To know the structure and/or process that fails, leading to lysis, septum maturation and cell lysis were studied by TEM (Fig. 7, E and F). In the WT after SS thickening, a new ring structure of dense material spanning from the PS and MTD to the wall surface appeared. We termed this structure dense ring (DR; Fig. 7 E, left). Cell separation started by controlled DR degradation, followed by gradual PS degradation, leaving a residual MTD called fuscannel (Johnson et al., 1973). The turgor pressure led the released SS to adopt the most stable spherical conformation (Fig. 7 E, left). In the absence of Bgs4, cell separation started with an uncontrolled cell wall degradation, probably because of a thick diffuse DR, leaving the PM exposed to the medium (Fig. 7 E, right). The exposed PM could not counteract the high internal pressure, causing the PM rupture and release of cytoplasm (Fig. 7 F, arrows). In no case was PS degradation detected, indicating that lysis occurs during cell wall degradation and before or at the start of PS degradation. These results show that Bgs4 is required for a correct septum–cell wall structure and to protect the cell from an excess of wall degradation at the start of cell separation.

Bgs4 is required to maintain the cell wall thickness and integrity during polarized growth

The pole lysis generated by Bgs4 absence occurred in both interphase and septated cells (Fig. 8 A, arrows), indicating a weakness of the pole wall that persists during cytokinesis. Interphase pole lysis was examined by CW staining and GFP-Bgs1 localization, which permitted discrimination of the growing poles. The lysis occurred at the old end (OE) during both monopolar and bipolar growth (Fig. 8, B [arrows] and C). The OE was located as the pole distant from the fission scar (Fig. 8 B). The OE supports most of the cell elongation, and hence the cell wall defect at this pole is stronger. The OE weakness also results in lysis after septation, probably because of the increase in the turgor pressure of the healthiest cell, transmitting the pressure to the sister cell, which will eventually lyse (Fig. 8 D, red arrowheads).

WT cells examined by TEM showed a uniform wall at both poles (Fig. 8 E). The absence of Bgs4 generated a very thin cell wall at the pole region (Fig. 8 F, red arrows). The thinness of the tip wall was restricted by its capacity to maintain the cell integrity. As a result, a thinner tip wall could not support the cell internal pressure, resulting in the cell wall and PM rupture and cytoplasm release (Fig. 8 F, right, red arrows).

The aforementioned cytokinesis and cell integrity defects were examined in the Bgs4-defective *cwg1-1* and *cwg1-2*

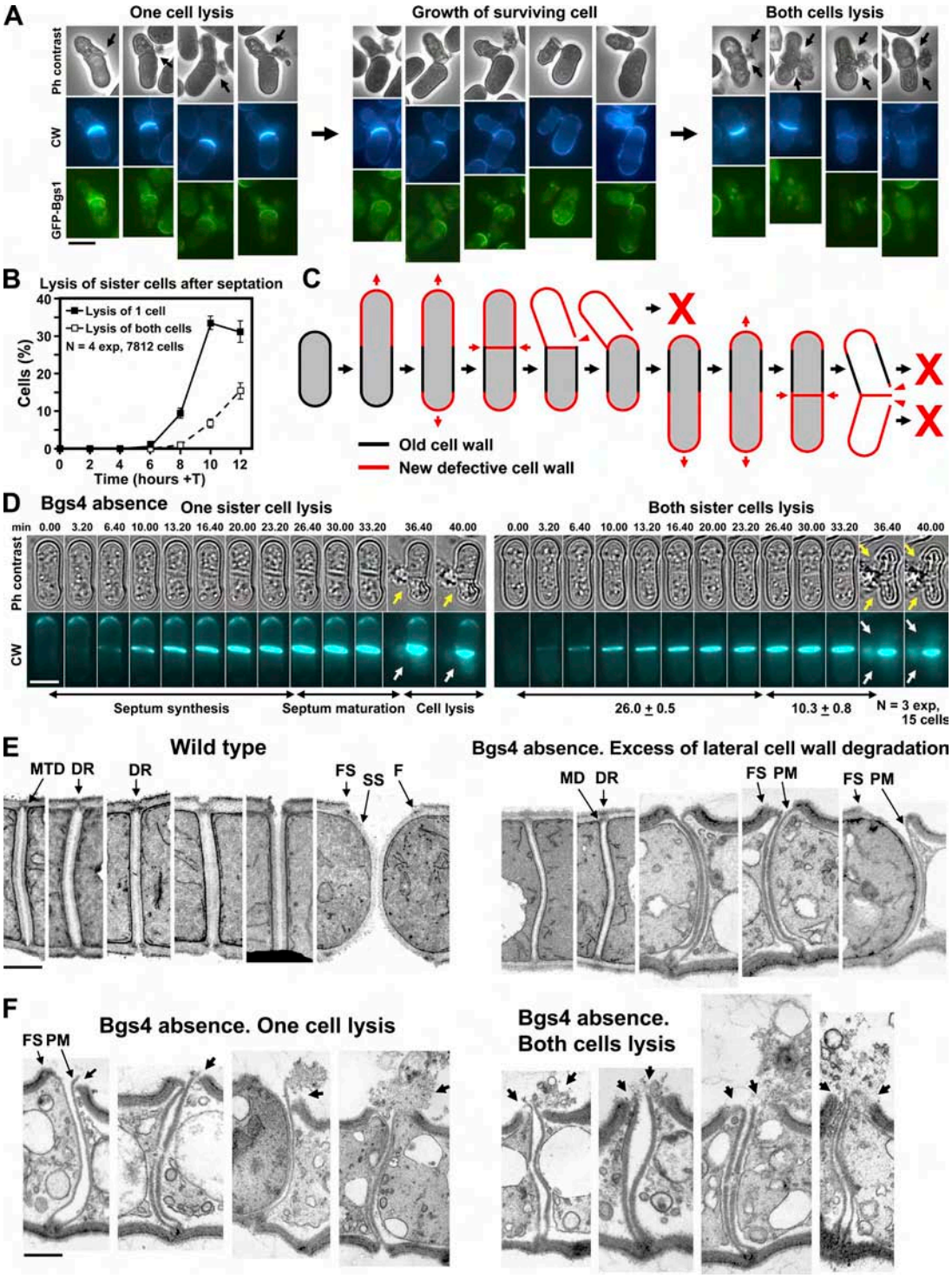

Figure 7. **Bgs4 is essential to protect the cell integrity from an excess of cell wall degradation at the start of cell separation.** (A–D) Bgs4 absence causes cell lysis and release of cytoplasm after septum maturation from either one or both sister cells. (A) The lysis in one cell (left) appears earlier, later increasing in both cells (right). Cells were grown as in Fig. 1 B. (B) Percentage of each cell lysis. Error bars indicate SD. (C) Model of differential cell lysis in one or both sister cells. The extension of asymmetric cell wall weakness caused by asymmetric cell growth (red arrows) and the septum position determine lysis (arrowheads) in one or both cells. (D) Cell lysis and cytoplasm release (arrow) from either one (left) or both (right) cells. Cells were grown as in Fig. 1 B and imaged by time-lapse. (E and F) TEM details of cell separation. (E) Controlled WT cell wall DR degradation and gradual PS degradation (left). Bgs4 absence causes an excess of cell wall degradation, leaving the PM exposed to the medium (right). (F) Cell lysis and cytoplasm release (arrow) at the start of cell separation, before PS degradation is detected. Cells were grown as in D. F, fuscannel; FS, fission scar. Bars: (cells) 5 µm; (septum details) 1 µm.

point mutants. As expected, loss of Bgs4 function led to phenotypes similar to those of Bgs4 absence (Fig. S5, A–E). Because other GS collaborate in SS, PS, and cell wall synthesis, the possible suppression of defects by overproduction of other GS was analyzed in both Bgs4-depleted and -defective strains. In no case did the overproduction of any other GS suppress

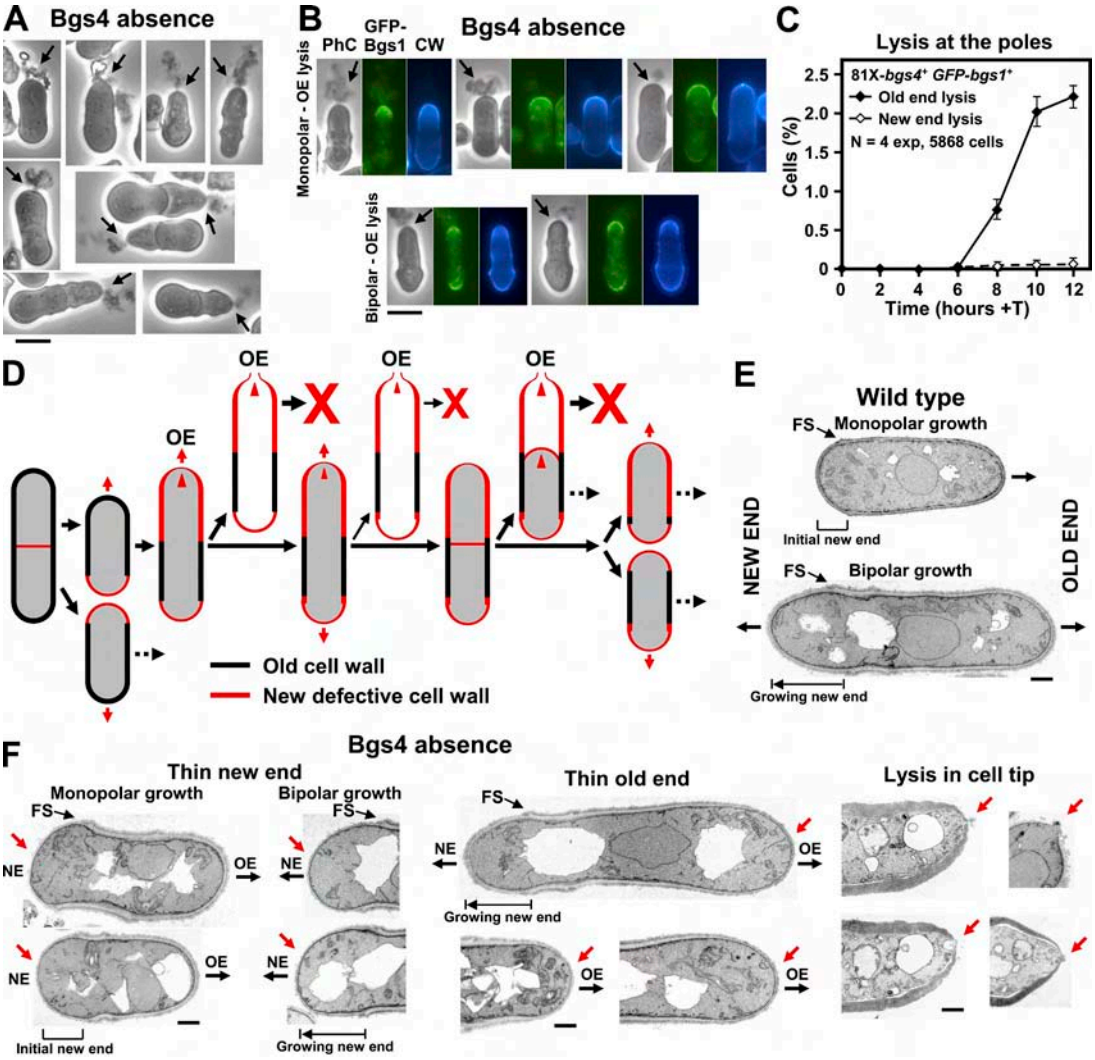

Figure 8. **Bgs4 is essential to maintain cell wall thickness and integrity at the poles.** (A) Bgs4 absence generates cell lysis and cytoplasm release from the poles (arrow) either during polar growth (top) or after septation (bottom). (B and C) Pole lysis occurs at the OE (arrow) during monopolar and bipolar growth. (A and B) Cells were grown as in Fig. 1 B. (C) Percentage lysis at each pole. Error bars indicate SD. (D) Model of lysis at the OE. Cell growth (red arrow) is mainly at the OE. The new defective cell wall cannot stand the internal pressure (arrowhead), resulting in pole lysis. After septum formation, the increase in internal pressure in a cell generates pole lysis of the sister cell. (E and F) Absence of Bgs4 causes a large pole cell wall thinning and lysis at the pole tip. (E) WT cell morphology and cell wall structure. (F) Bgs4 absence generates a thin cell wall (red arrow) in both new end (close to FS) and OE. A thinner tip wall results in cell lysis and cytoplasm release (right, red arrow). Cells were grown as in A. FS, fission scar; NE, new end. Bars: (A and B) 5 µm; (E and F) 1 µm.

the phenotypes promoted by the Bgs4 B-BG absence, and it even increased the lethality of *cwg1-1* and *cwg1-2* mutants (Fig. S5 F). This suggests that no other glucan can compensate the defect because of B-BG absence. However, the fact that compensatory mechanisms were able to form remedial SS and stable survivors (unpublished data) suggests that a specific induction and/or repression level of combined GS could compensate the lethal Bgs4 B-BG absence.

Discussion

CAR contraction is a well conserved process in fungi and animal cells (Bathe and Chang, 2010; Lee et al., 2012). How fungal CAR constriction is coordinated with the late cytokinesis steps of septum synthesis and how the synthases cooperate to assemble the septum have just started to be understood (Sipiczki, 2007; Cortés et al., 2012). Fission yeast contains different essential GS with specific roles in cytokinesis. However, the role of Bgs4 in the cell wall and septum remains unknown (Cortés et al., 2005). We have studied the septation process of *S. pombe* in depth and found interesting remedial septation mechanisms for cell survival (Fig. 9 A). Cell separation is critical and hence the result will differ, depending on the septation mechanism (Fig. 9 B).

Bgs4 β(1,3)glucan is necessary for correct CAR positioning in the cell middle and for coupling septum synthesis to PM extension and CAR contraction

Our data show for the first time that extracellular B-BG has a role in the CAR function. In the absence of B-BG the CAR is often oblique assembled, sliding in the cell middle until septum

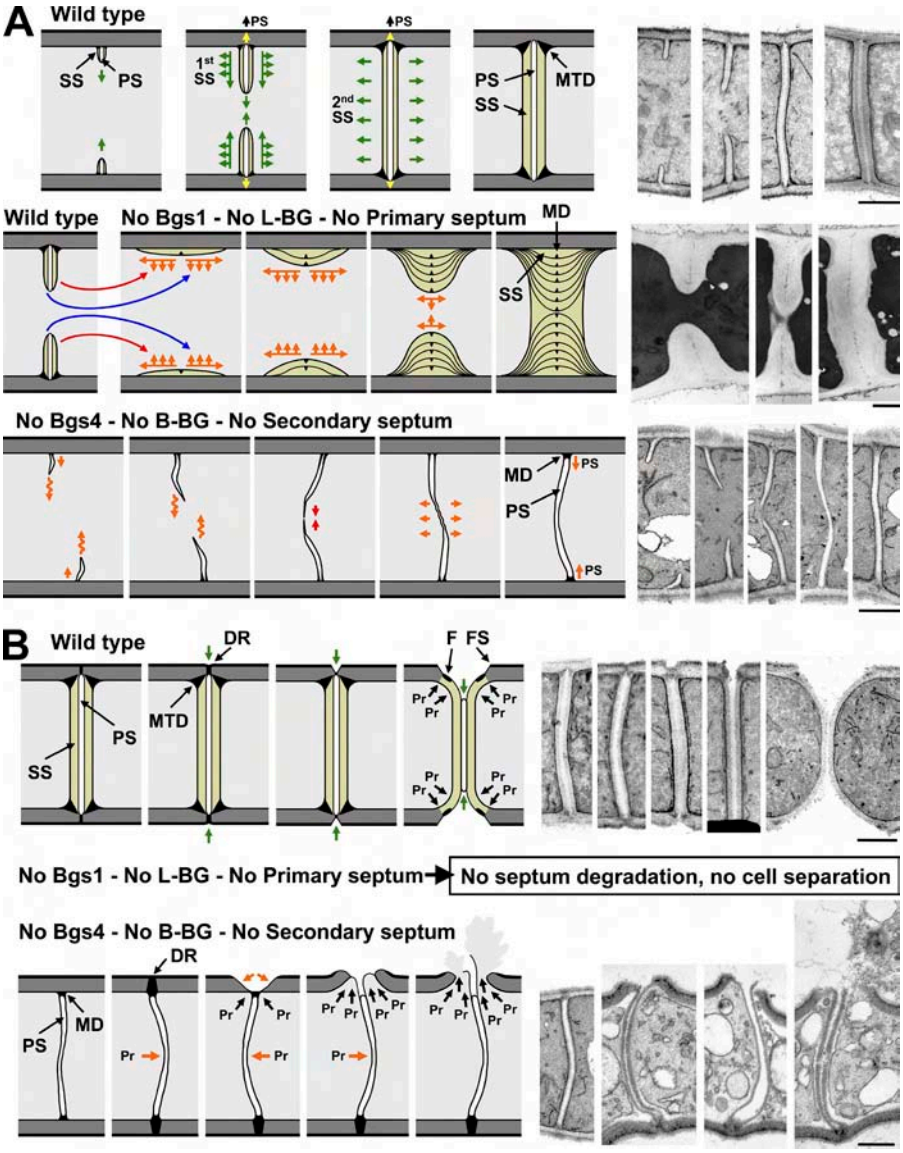

Figure 9. **Models of the septation process and alternative septations of fission yeast.** (A) WT septation (top). Simultaneous coordinated synthesis (arrow) of PS (perpendicular to cell wall) and SS (parallel to PS) form a three-layered septum. Septum maturation proceeds by PS anchorage into the cell wall (yellow arrow) and a second round of SS synthesis. (middle) Septation in Bgs1 absence. The SS is synthesized parallel to the cell wall. The septum grows by successive parallel SS depositions (orange arrow). The MTD changes to a septum medial position, forming a dotted line of MD in the SS layers (Cortés et al., 2007). (bottom) Septation in Bgs4 absence. CAR and septum are oblique positioned in the cell middle. The septum grows as a weak twisted and misdirected PS (wavy arrows) that is delayed and uncoupled from CAR and PM ingression (red arrows). After septum completion, the defective middle region is repaired with new PS (orange arrows) and the PS is retracted from the cell wall. (B) WT cell separation (top). Controlled cell wall DR and PS degradation (arrow) and the osmotic pressure that curves the SS to the stable conformation ensure a safe separation. In Bgs1 absence, there is no cell separation (middle). Cell separation and lysis in Bgs4 absence (bottom). Uncontrolled cell wall DR degradation (arrow) leaves the PM exposed to the medium. Then the turgor pressure generates the PM rupture and cytoplasm release. F, fuscannel; FS, fission scar; Pr, turgor pressure. Bars, 1 µm.

synthesis initiation fixes CAR and septum position to the cell wall. We discarded a Bgs4 defect because it is not present during CAR positioning and sliding, appearing after septum initiation (Cortés et al., 2005). However, the cell wall B-BG absence generated in previous cycles is a defect present during CAR formation and sliding. CAR sliding has been described in the combined absence of microtubules or anillin-like Mid1 function with the absence of septum synthesis start (Pardo and Nurse, 2003; Huang et al., 2008). In these cases the defect was caused in the CAR, whereas in our case the defect is caused by cell wall B-BG absence. Supporting our finding of the important role of cell wall B-BG in CAR function, spherical protoplasts devoid of cell wall show unstable CAR sliding toward the poles (Mishra et al., 2012), whereas spherical mutants with cell wall form stable CAR and septa (Chang et al., 1994; Verde et al., 1995; Sipiczki et al., 2000).

Despite our knowledge of cytokinesis, little is known about how extracellular signals communicate with intracellular events. The extracellular cell wall must be connected to the PM and CAR, and here we show that B-BG is crucial for this interaction. As B-BG is external, the CAR must interact with B-BG through PM proteins connecting both sides. Bgs and Ags1 proteins cannot be candidates for such an interaction because all appear in the middle much later than the time of CAR defects. Candidates could be the scaffold protein anillin, G protein–coupled receptors, or ECM proteins, as suggested in animal cells (Almonacid and Paoletti, 2010; Hynes and Naba, 2012; Liu et al., 2012; Lu et al., 2012; Rincón and Paoletti, 2012; Zhang et al., 2012). In fact, proteins and polysaccharides of the animal ECM (functional equivalent of fungal cell wall) have been shown to be critical for cytokinesis (Hwang et al., 2003; Mizuguchi et al., 2003; Olson et al., 2006; Izumikawa et al., 2010; Jordan et al., 2011; Xu and Vogel, 2011). However, how the ECM is coupled to the CAR and how it affects the CAR function remain largely unknown.

Our results show a surprising separation between slower PS synthesis and faster CAR and PM ingression, indicating that the pushing force of PS synthesis is not necessary for CAR and

PM progression (Johnson et al., 2005). More surprisingly, the contraction rate of uncoupled CAR and PM is faster than normal, suggesting that in normal coupled cytokinesis the synthesis rate of attached PS restricts CAR and PM ingression rates. Moreover, our data show that septation can progress with a defective CAR pulling force. In the absence of B-BG, the initial septa are twisted and bent and larger septa appear misdirected, indicating a relaxed CAR without the tensile pulling force necessary to maintain the growing septum straight. These results suggest that cytokinesis can progress and be completed without or with a defective pushing force of septum synthesis and/or pulling force of CAR contraction, with the help of PM extension by the addition of membrane vesicles. In fact, it has been described that cytokinesis can be completed with defective CAR, but to date this has not been reported with delayed PS deposition (Pollard, 2010; Balasubramanian et al., 2012; Proctor et al., 2012).

It has been suggested that septum synthesis provides the primary force for the last cytokinesis steps based on the fact that in LatA-treated cells, septum synthesis can continue and be completed without the CAR (Proctor et al., 2012). However, only septa above 50% in length progress and complete septation, and the progression rate decreases to 30%, thus suggesting an important role for the CAR in the overall septum ingression process. In addition, it is possible that in these LatA-treated cells other CAR components more stable than actin could maintain a residual CAR that might help in the final septum progression (Naqvi et al., 1999; Wu et al., 2003). In Bgs4-depleted cells, the CAR structure is not altered but Bgs4 B-BG and septum are, indicating that when the CAR is intact the septum pushing force is not so critical. However, the misdirected CAR and PM progression suggests that not only the PS pushing force but also the CAR contraction force is defective, unable to maintain a straight septum progression. In these conditions, the PM and CAR ingression rate increased to 127% of WT, suggesting that when detached from the PS, the PM advance proceeds faster, whereas the attached CAR cannot constrict at similar rate, resulting in a larger and relaxed misdirected CAR structure, in agreement with the proposed low contractile force of the CAR (Proctor et al., 2012). That the septa are always completed indicates that the CAR constriction force is still able to finally correct the misdirected progression. In the absence of B-BG, the septa present a very sharp PM tip, suggesting that if some material is deposited between PM and PS the septum pushing force would be limited. In addition, the observation of septa with advancing PS but complete PM with no space for deposited material (Fig. 4 F) suggests that the PM can progress without pushing septum material. Collectively, these results suggest that both CAR and septum synthesis collaborate in a normal septum formation. Septum progression is necessary to complete a septum wall structure, and the CAR is essential for septation start and at least first-half progression and as a safety closing belt mechanism for a straight progression.

Previously, we have found interesting the convergent similarities between the structure and function of fission yeast PS and plant cell plate during cytokinesis (Cortés et al., 2007, 2012). Our current observations reveal important convergent similarities between fungal and animal cytokinesis, with a fungal cell wall B-BG required for connecting cell wall and CAR during cytokinesis and ECM polysaccharides required for animal cytokinesis (White and Bednarek, 2003; Mizuguchi et al., 2003; Olson et al., 2006; Izumikawa et al., 2010), suggesting that the extracellular cell wall is an evolutionarily highly conserved component of eukaryotic cytokinesis.

Bgs4 is essential for SS formation and PS completion

We found that Bgs4 B-BG is responsible for SS assembly (Fig. 9 A). A similar function has been described for Ags1 (Cortés et al., 2012), indicating that both B-BG and α-glucan are necessary but not sufficient for SS formation. Analysis of reverting protoplasts suggests that the primary wall formation step is the assembly of β-glucan microfibrils, whereas α-glucan might be involved in glucan bundle formation (Osumi et al., 1989; Konomi et al., 2003). In fact, α-glucan is required for adhesion (Cortés et al., 2012). Also, Bgs4 or Ags1 absence causes the induction of remedial SS and cell survival (Cortés et al., 2012; unpublished data). However, remedial SS appear later in the absence of Bgs4, suggesting different compensatory mechanisms. In fact, Rho1 GTPase regulates both α- and β-glucan synthesis, whereas Rho2 mainly regulates α-glucan synthesis (Pérez and Cansado, 2010; Perez and Rincón, 2010). Evaluation of the compensatory mechanisms will require further analysis of Ags1 and Bgs subunits.

We show that although the L-BG is responsible for the PS structure, it needs the participation of B-BG. Absence of Bgs4 causes PS thinning in the last stages of PS synthesis, indicating that B-BG is needed to reinforce the growing PS edge. In this sense, Bgs4 absence generates flexible oscillating septa. This flexibility is not caused by the absence of SS because it is not observed in the absence of Ags1 (Cortés et al., 2012), indicating that B-BG specifically confers the septum rigidity. Similarly to *Saccharomyces cerevisiae* chitin, *S. pombe* B-BG could provide the septum rigidity by binding to L-BG or α-glucan (Hartland et al., 1994). Indeed, it has been suggested that L-BG association with B-BG or α-glucan is critical for PS assembly (Cortés et al., 2007).

Bgs4 is essential for cell integrity at the start of cell separation

S. pombe is an excellent model for cell integrity studies because of its critical cell separation process (Roncero and Sánchez, 2010; Cortés et al., 2012). Cell separation starts by controlled cell wall degradation and the DR could be important for this process (Fig. 9 B). L-BG has been shown to be essential for cell separation (Cortés et al., 2007). Thus, the DR could be a structure rich in L-BG, directing the degradation to this structure, whereas B-BG could accumulate around the DR to protect the cell wall. Ags1-depleted cells also display cell lysis during cell separation (Cortés et al., 2012). It will be interesting to evaluate whether Bgs4 and Ags1 cooperate in safe cell separation.

Materials and methods

Strains and culture conditions

The *S. pombe* strains used in this study are listed in Table S1. *bgs4Δ::ura4*$^+$ p81XH-*bgs4*$^+$ strain 498 (*his3*$^+$ selection) has been described previously (Cortés et al., 2005). This strain contains *bgs4*$^+$ expressed under the control of the 81X version (low expression) of the thiamine-repressible *nmt1*$^+$ promoter (Moreno et al., 2000).

81X-*bgs4*$^+$ strain 1288 (Leu$^-$, Ura$^+$, and His$^+$) contains the *bgs4*Δ*::ura4*$^+$ deletion and a single p81XH-*bgs4*$^+$ copy integrated adjacent to the *his3-Δ1* locus. This strain was generated from strain *bgs4*Δ*::ura4*$^+$ p81XH-*bgs4*$^+$ by continuous growth in minimal medium (MM) with histidine, colony isolation, and selection of clones that maintain the His$^+$ phenotype. Next, the selected clones were analyzed by genetic cross with strain 285 (WT, Leu$^-$, Ura$^-$, and His$^-$) and tetrads analysis. Clones that segregated 2His$^+$:2His$^-$, indicative of 81XH-*bgs4*$^+$ integration, were selected. Finally, these clones were analyzed by genetic cross with strain 420 (WT, Leu$^-$, Ura$^-$, and His$^+$) and tetrad analysis. The clones that showed a 4His$^+$:0His$^-$ segregation, indicative of a correct 81XH-*bgs4*$^+$ integration adjacent to the *his3-Δ1* locus, were selected. All the 81X-*bgs4*$^+$ clones exhibited a strong lytic phenotype in the presence of thiamine (repressed conditions) and a WT phenotype in its absence (induced conditions). Other 81X-*bgs4*$^+$ strains were made from strain 1288 either by tetrad dissection or by random spore analysis by selecting against the corresponding parental auxotrophies. 81X-*GFP-bgs4*$^+$ strain 1493 (Leu$^-$, Ura$^+$, His$^+$, and Ade$^-$) contains the *bgs4*Δ*::ura4*$^+$ deletion and a single p81XH-*GFP-bgs4*$^+$ copy integrated adjacent to the *his3-Δ1* locus. This strain was made following a protocol similar to that described for strain 81X-*bgs4*$^+$.

GFP-bgs1$^+$, *GFP-bgs3*$^+$, *GFP-bgs4*$^+$, and *ags1*$^+$*-GFP* strains 520, 1217, 561, and 3166, respectively, have already been described (Cortés et al., 2002, 2005, 2007, 2012). These strains contain the *bgs1*Δ*::ura4*$^+$, *bgs3*Δ*::ura4*$^+$, *bgs4*Δ*::ura4*$^+$, and *ags1*Δ 3′UTR$_{ags1+}$::*ags1*$_{3704\text{-}7233}$*:ura4*$^+$ deletions and an integrated copy of SmaI-cut pJK-*GFP-bgs1*$^+$, PacI-cut pJK-*GFP-bgs3*$^+$, StuI-cut pJK-*GFP-bgs4*$^+$, and AgeI-cut pJK-*ags1*$_{1\text{-}6267}$*-GFP* (*leu1*$^+$ selection), which direct their integrations at the SmaI site of the *bgs1*$^+$ promoter sequence (nt −748) adjacent to *bgs1*Δ*::ura4*$^+$, the PacI site of the *bgs3*$^+$ promoter sequence (nt −1857) adjacent to *bgs3*Δ*::ura4*$^+$, the StuI site of the *bgs4*$^+$ promoter sequence (nt −1320) adjacent to *bgs4*Δ*::ura4*$^+$, and the AgeI site of the *ags1*$^+$ coding sequence (nt 6025) in *ags1*Δ 3′UTR$_{ags1+}$::*ags1*$_{3704\text{-}7233}$*:ura4*$^+$, respectively. *2xGFP-bgs1*$^+$ strain 1731 was made as described for the *GFP-bgs1*$^+$ strain (Cortés et al., 2002) and contains an integrated copy of SmaI-cut pJK-*2xGFP-bgs1*$^+$ (*leu1*$^+$ selection), which directs its integration at the SmaI site adjacent to *bgs1*Δ*::ura4*$^+$, at position −748 of the *bgs1*$^+$ promoter sequence. Likewise, *2xRFP-bgs1*$^+$ strain 1780 contains an integrated copy of SmaI-cut pJK-*2xRFP-bgs1*$^+$ (tdTomato variant [Shaner et al., 2005]) at position −748 of the *bgs1*$^+$ promoter sequence. *2xRFP-bgs1*$^+$ *GFP-bgs3*$^+$ strain 3332 was made by a genetic cross between strains 1780 (*2xRFP-bgs1*$^+$, Leu$^+$, Ura$^+$, and His$^-$) and 1217 (*GFP-bgs3*$^+$, Leu$^+$, Ura$^+$, and His$^-$), tetrad dissection, and analysis of RFP-Bgs1 and GFP-Bgs3 localizations.

2xGFP-bgs1$^+$ 81X-*bgs4*$^+$ strain 2300 was made by a genetic cross between strains 1731 (*2xGFP-bgs1*$^+$, Leu$^+$, Ura$^+$, His$^-$, and Ade$^+$) and 1366 (81X-*bgs4*$^+$, Leu$^-$, Ura$^+$, His$^+$, and Ade$^-$) and random spore selection of Leu$^+$ (*2xGFP-bgs1*$^+$), Ura$^+$ (*bgs1*Δ*::ura4*$^+$ and *bgs4*Δ*::ura4*$^+$), and His$^+$ (81X-*bgs4*$^+$) clones, followed by analysis of GFP-Bgs1 localization and lysis promoted by *bgs4*$^+$ repression in the presence of thiamine. Similarly, other 81X-*bgs4*$^+$ strains were made by genetic cross between the corresponding parental strains, random spore selection of Leu$^+$ (GFP- or RFP-tagged proteins), Ura$^+$ (*bgs4*Δ*::ura4*$^+$ and other *ura4*$^+$ deletions), and His$^+$ (81X-*bgs4*$^+$) clones, and analysis of the corresponding GFP or RFP localization and lysis induced by *bgs4*$^+$ repression.

Standard complete yeast growth (YES), selective (MM) with the appropriate supplements, and sporulation media (Egel, 1984; Alfa et al., 1993) have been described. Cell growth was monitored by measuring the A_{600} of early log-phase cell cultures in a Junior II spectrophotometer (A_{600} 0.15 = 1 × 10^7 cells/ml; Coleman). The determinations were performed in two different clones of the same strain in three independent experiments. For serial dilution drop tests of growth, early log-phase cells growing at 25 or 30°C were adjusted to 10^7 cells/ml and then serially diluted 1:10. The different dilutions were spotted onto MM, YES, and MM + thiamine plates, incubated for 2–4 d at the indicated temperatures, and photographed. The test was repeated in two independent experiments. General procedures for yeast and bacterial culture and genetic manipulations (genetic crosses, tetrad dissection and analysis, random spore selection and analysis, yeast and bacterial transformations, plasmid manipulations, etc.) were performed as described previously (Moreno et al., 1991; Sambrook and Russell, 2001).

Plasmids and DNA techniques

p81XH-*bgs4*$^+$ has been described previously (Cortés et al., 2005). This plasmid contains the *bgs4*$^+$ ORF with XhoI and PstI sites inserted by site-directed mutagenesis just before the start codon and just after the TAG stop codon of *bgs4*$^+$, respectively, cloned into XhoI-PstI of pJR2-81XH (*his3*$^+$ selection and 81X version of the thiamine-repressible *nmt1*$^+$ promoter; Moreno et al., 2000). The resulting *S. pombe* strain *bgs4*Δ p81XH-*bgs4*$^+$ displayed a lethal lytic phenotype under repressed conditions (presence of thiamine) and the WT phenotype in induced conditions (absence of thiamine). The *bgs4*$^+$ shut-off phenotype of strains containing multicopy p81XH-*bgs4*$^+$ was heterogeneous and the appearance of revertant or attenuated clones was detected. To obtain a strain with a more uniform, more stable, and faster *bgs4*$^+$ shut-off phenotype, which could be useful to study the Bgs4 absence effect, a *bgs4*Δ strain with an integrated 81X-*bgs4*$^+$ single copy was made (see previous section). As expected, lysis and cell growth arrest appeared earlier in the 81X-*bgs4*$^+$ strain because of its reduced *bgs4*$^+$ expression and still maintained the WT phenotype in induced conditions.

p81XH-*GFP-bgs4*$^+$ is pJR2-81XH containing the XhoI-PstI *GFP-bgs4*$^+$ ORF with the *GFP* inserted in-frame at base 970 (amino acid 324), as described previously to obtain a functional GFP-Bgs4 fusion (Cortés et al., 2005). Likewise, a *bgs4*Δ strain with an integrated 81X-*GFP-bgs4*$^+$ single copy was made (see previous section). The lysis and cell growth arrest of 81X-*GFP-bgs4*$^+$ strain was similar to that of 81X-*bgs4*$^+$.

Plasmids pJK-*GFP-bgs1*$^+$, pJK-*GFP-bgs3*$^+$, pJK-*GFP-bgs4*$^+$, and pJK-*ags1*$_{1\text{-}6267}$*-GFP* have been described elsewhere (Cortés et al., 2002, 2005, 2007, 2012). These plasmids are the integrative plasmid pJK148 (*leu1*$^+$ selection) with a 9.6-kb ApaI-SpeI *GFP-bgs1*$^+$, 10.4-kb SpeI-SpeI *GFP-bgs3*$^+$, 9.6-kb PstI-NheI *GFP-bgs4*$^+$, and 9.9-kb EcoRI-NheI *ags1*$_{1\text{-}6267}$*-GFP* fragment, respectively. pJK-*2xGFP-bgs1*$^+$ contains a 10.3-kb *2xGFP-bgs1*$^+$ fragment with a 1.5-kb tandem of two *GFP* sequences cloned in-frame and separated by a 12-alanine linker to make a more flexible 2xGFP epitope. pJK-*2xRFP-bgs1*$^+$ contains a 10.2-kb *2xRFP-bgs1*$^+$ fragment with the 1.4-kb tandem dimer tdTomato variant of the monomeric mRFP1 protein (Shaner et al., 2005; provided by R.Y. Tsien, University of California, San Diego, La Jolla, CA).

Plasmids pAL-*bgs1*$^+$ and pAL-*bgs4*$^+$ have been described previously (Cortés et al., 2002, 2005). These plasmids are the multicopy plasmid pAL-KS+ (*S. cerevisiae LEU2* selection) with a 7.2-kb HindIII–SpeI *bgs1*$^+$ and an 8.8-kb PstI–NheI *bgs4*$^+$ fragment, respectively. Similarly, pAL-*bgs3*$^+$ and pAL-*ags1*$^+$ contain a 9.7-kb SpeI–SpeI *bgs3*$^+$ and an 11.2-kb EcoRI–NruI fragment, respectively (Cortés et al., 2007, 2012). These multicopy plasmids contain the corresponding ORF and its native promoter sequence, and were used for overexpression studies.

Plasmids p41X-*bgs1*$^+$, p41X-*bgs3*$^+$, p41X-*bgs4*$^+$, and p41X-*ags1*$^+$ are the multicopy thiamine-repressible plasmid pJR-41XL (Moreno et al., 2000) with the 5.2-kb *bgs1*$^+$ ORF, 5.5-kb *bgs3*$^+$ ORF, 5.9-kb *bgs4*$^+$ ORF, and 7.2-kb *ags1*$^+$ ORF sequence, respectively. Induced and repressed expression levels of the 41X plasmid are 10–50-fold higher than those of the 81X version and 5–20-fold lower than those of the 3X version. Higher overexpression of these ORFs with the 3X version is toxic for the cell. Therefore, the 41X plasmid was selected for overexpression studies at both induced and repressed expression levels.

Immunoblot analysis

Early log-phase cells (10^9 cells) expressing the different tagged proteins were harvested (1,500 *g*, 5 min, 4°C), washed twice with cold buffer (1 mM EDTA and 1.2 M sorbitol, 4°C), suspended in 100 µl of lysis buffer (50 mM Tris-HCl, pH 7.5, 1 mM EDTA, 150 mM NaCl, 0.1% Triton X-100 containing 1 mM phenylmethylsulphonylfluoride, and 2 µg/ml aprotinin, leupeptin, and pepstatin), and broken with glass beads (FastPrep FP120, 3 × 15 s, speed of 5.5 [MP Biomedicals; Thermo Fisher Scientific]). The total cell extracts were collected by bottom-tube perforation and centrifugation (5,000 *g*, 20 s, 4°C). The cell extracts were resuspended, centrifuged (21,000 *g*, 5 min, 4°C), and homogenized again in the same supernatant. This step improved the disaggregation and immunodetection of membrane proteins from total cell extracts. Finally, samples were diluted with 2× loading buffer (2× is 100 mM Tris-HCl, pH 6.8, 2% SDS, 2% 2-mercaptoethanol, 25 mM EDTA, 20% glycerol, and 0.05% bromophenol blue) and stored at −80°C. The protein concentration of the loading samples was quantified by the Bradford assay (Bio-Rad Laboratories). Samples (80 µg of total protein) were heated at 65°C for 5 min and centrifuged (20,000 *g*, 20 s) to precipitate the insoluble material. Proteins were subjected to 3–8% Tris-Acetate SDS-PAGE (NuPAGE; Invitrogen), blotted onto Immobilon-P membranes (EMD Millipore), and probed with monoclonal JL-8 anti-GFP (1:2,000; Living colors; Takara Bio Inc.) or monoclonal B-5-1-2 anti–α-tubulin (1:10,000; Sigma-Aldrich) antibodies. Immunodetection was performed with anti–mouse horseradish-conjugated antibody (1:10,000) and the ECL detection kit (GE Healthcare). Protein amounts were quantified by chemiluminescence with a ChemiDoc XRS System (Bio-Rad Laboratories) and Quantity One software (Bio-Rad Laboratories). Total cell extracts and Western blots were repeated from three to five times for each experiment. The data from the Western blots were quantified and the mean values of the relative amount of each protein were calculated from three to five independent total cell extracts.

Labeling and fractionation of cell wall polysaccharides

[^{14}C]Glucose labeling and fractionation of cell wall polysaccharides were performed essentially as described previously (Cortés et al., 2012). Early log-phase cells incubated in MM + 1.2 M sorbitol were diluted with the same medium (with 20 µg/ml thiamine for cells repressing *bgs4*$^+$) and supplemented with D-[U-^{14}C]glucose (6 µCi/ml; Hartmann Analytic) 4 h before harvesting. The cells (early log-phase) were collected at the indicated times. Total glucose incorporation was monitored by measuring radioactivity in trichloroacetic acid–insoluble material. Cells were harvested, supplemented with unlabeled cells as the carrier, washed twice with 1 mM EDTA, and broken with glass beads (FastPrep FP120, 3 × 20 s and speed of 6.0). Cell walls were purified by repeated washing and differential centrifugation (once with 1 mM EDTA, twice with 5 M NaCl, and twice with 1 mM EDTA) at 1,500 *g* for 5 min. Purified cell walls were heated at 96°C for 20 min and [^{14}C]glucose incorporation into the cell wall was monitored.

Cell wall samples were extracted with 6% NaOH for 60 min at 80°C and neutralized with acetic acid. Precipitation of the galactomannan fraction from the neutralized supernatant was performed with Fehling´s reagent by adding 5 mg of unlabeled yeast mannan as the carrier (stock of 50 mg/ml in water [Sigma-Aldrich], as described previously (Algranati et al., 1966). Fehling´s reagent was freshly prepared for each experiment by adding one volume of reagent B (3.5% $CuSO_4$) to one volume of reagent A (17.3% potassium sodium tartrate dissolved in 12.5% KOH). In brief, four volumes of Fehling´s reagent were added to the samples, mixed, and left overnight at 4°C to precipitate the galactomannan. After centrifugation at 1,500 *g* for 10 min, the pellets were washed with Fehling´s reagent and solubilized in 20–40 µl of 6N HCl. Then, 100 µl of 50 mM Tris-HCl, pH 7.5, was added and the radioactivity of the solutions was measured in a scintillation counter (Beckman Coulter) and considered the galactomannan fraction.

Other samples of cell wall suspension were incubated with Zymolyase 100T (25 µg of enzyme and 1/20 volume of cell wall suspension; AMS Biotechnology) in 50 mM citrate-phosphate buffer, pH 5.6, for 24 h at 37°C. Samples without enzyme were included as a control. After incubation, samples were centrifuged and washed with the same buffer. One ml of 10% trichloroacetic acid was added to the pellets, filtered in Whatman GF/C glass fiber filters (2 × 2 ml of 10% trichloroacetic acid and 2 ml of ethanol), and their radioactivity levels were measured in a scintillation counter. The Zymolyase 100T pellets were considered the α-glucan fraction, and the supernatants were the β-glucan-plus-galactomannan fraction. β-Glucan was calculated as radioactivity remaining after subtraction of galactomannan and α-glucan from total cell wall incorporation. All determinations were performed in duplicate, and data for each strain were calculated from three independent cultures.

Microscopy techniques

For cell wall staining, early log-phase cells grown in MM + 1.2 M sorbitol (MM+S; with 20 µg/ml thiamine for cells repressing *bgs4*$^+$) at 30°C or in YES at 25°C and shifted to 37°C for 5–7 h (thermosensitive mutant cells) were concentrated (1,000 *g*, 1 min) and visualized directly by adding a solution of CW (50 µg/ml final concentration [Blankophor; Blankophor GmbH & Co.]; Fluorescent Brightener 28 [Sigma-Aldrich]) to the sample and using the appropriate filter. GFP and RFP were directly visualized from early log-phase cells by using the appropriate filters. Images were obtained with a fluorescence microscope (DM RXA; Leica), a PL APO 63×/1.32 oil PH3 objective, a digital camera (DFC350FX; Leica), and CW4000 cytoFISH software (Leica). Images were processed with Photoshop CS2 software (Adobe). All the analyses were repeated in three to four independent experiments and representative images of the analyzed phenotype were indistinctly selected from the experiments. Graphical data were calculated from four independent experiments. The number of experiments and of total CAR, septa, or cells analyzed is shown in each case.

For time-lapse imaging, 0.3–0.6 ml of log-phase cells grown in MM+S (with 20 µg/ml thiamine for cells repressing *bgs4*$^+$) at 30°C or in YES at 25°C and shifted to 37°C for 5–6 h were collected by low-speed centrifugation (1,000 *g*, 1 min), resuspended in 300 µl of the same media containing CW (5 µg/ml final concentration), and placed in a well from a µ-Slide 8 well (80821-Uncoated; Ibidi) previously coated with 10 µl of 1 mg/ml soybean lectin (L1395; Sigma-Aldrich). Time-lapse experiments were made at 30°C (MM+S) or 37°C (YES) by acquiring epifluorescence and/or phase-contrast cell images in single planes and 1 × 1 binning on an inverted microscope (IX71; Olympus) equipped with a PlanApo 100×/1.40 IX70 objective and a Personal DeltaVision system (Applied Precision). Images were captured using CoolSnap HQ2 monochrome camera (Photometrics) and SoftWoRx 5.5.0 imaging software (Applied Precision). In some cases, time-lapse images were restored and corrected by 3D Deconvolution (conservative ratio; 10 iterations and medium noise filtering) through SoftWoRx imaging software. Subsequently, images were processed (color, brightness, contrast, and/or sharpness) with ImageJ (National Institutes of Health) and Photoshop CS2 software. All the time-lapses were repeated in two to three independent experiments. The data were calculated from two to three independent experiments. The number of experiments and of total cells analyzed is shown in each case.

TEM

Early log-phase cells were fixed with 2% glutaraldehyde EM (GA; Electron Microscopy Science) in 50 mM phosphate buffer, pH 7.2, and 150 mM NaCl (PBS) for 2 h at 4°C, post-fixed with 2% potassium permanganate for 1 h at room temperature, dehydrated in acetone, and embedded in epoxy resin. Ultrathin sections were examined with a Jam-1010 electron microscope (Jeol).

Online supplemental material

Fig. S1 shows that absence of Bgs4 promotes cell lysis and cytoplasm release during both cytokinesis and polarized growth. Fig. S2 shows that Bgs4 is required for CW-stained PS completion but not for CAR contraction and septum PM closure. Fig. S3 shows that Bgs4 and its β(1,3)glucan are required for correct and stable CAR positioning in the cell middle and for correct straight CAR constriction and septum ingression. Fig. S4 shows that Bgs4 is essential for coupling septum formation to CAR contraction, to confer the septum rigidity, and to protect the cell integrity at the start of cell separation. Fig. S5 shows that the Bgs4-defective *cwg1-1* and *cwg1-2* mutants show defects as those in the absence of Bgs4. The defects cannot be compensated by any other GS. Video 1 shows the formation of an oblique CAR and septum of two dividing Bgs4-depleted cells. Video 2 shows the formation of an altered CAR but normal septum of two dividing Bgs4-depleted cells. Video 3 shows the formation of an oblique CAR and septum of four cells expressing the *cwg1-2* mutation of *bgs4*$^+$. Video 4 shows the formation of a misdirected CAR and septum of five cells expressing the *cwg1-1* mutation of *bgs4*$^+$. Video 5 shows the coordinated CAR contraction and septum formation of a WT cell. Video 6 shows the uncoupling between CAR contraction and the slower septum formation of three Bgs4-depleted cells. Video 7 shows the formation of a rigid and straight septum and the progressive cell separation of two WT cells. Videos 8 and 9 show the formation of a flexible and oscillating curved septum with two and four waving cycles, respectively, of four Bgs4-depleted cells. Video 10 shows the cell lysis and release of cytoplasm from either one or both sister cells at the start of cell separation of three dividing Bgs4-depleted cells. Table S1 lists the fission yeast strains used in this study. Online supplemental material is available at http://www.jcb.org/cgi/content/full/jcb.201304132/DC1.

This paper is dedicated to Angel Durán, who taught us much about yeast, on the occasion of his retirement and his contributions in the field of yeast cell wall morphogenesis. We thank E. Cabib for comments on the manuscript; C. Sacristán for technical help with the drop tests; R. Tsien for RFP-containing plasmids; and P. Munz, T. Pollard, V. Simanis, M. Balasubramanian, Y. Sánchez, C. Shimoda, and R. Martín-García for strains.

We thank the Ramón Areces Foundation for Instituto de Biología Funcional y Genómica financial support. J. Muñoz, M. Ramos, and J.A. Clemente-Ramos acknowledge support by fellowships from Junta de Castilla y León, Consejo Superior de Investigaciones Científicas, and Ministerio de Ciencia e Innovación (MICINN; Spain), respectively; J.C.G. Cortés by a "Juan de la Cierva" contract from MICINN; and I.M. Martins by a fellowship from Fundação para a Ciência e a Tecnologia (Portugal). This work was supported by grants BIO2009-10597, BFU2010-15641, and BIO2012-35372 (MICINN), CSI376A12-2 (Junta de Castilla y León), and OTKA 101323 (Hungarian Scientific Research Fund).

Submitted: 22 April 2013
Accepted: 19 September 2013

References

Alfa, C., P. Fantes, J. Hyams, M. McLeod, and E. Warbrick. 1993. Experiments with fission yeast: a laboratory course manual. Cold Spring Harbor Laboratory Press, Cold Spring Harbor, NY. 186 pp.

Algranati, I.D., N. Behrens, H. Carminatti, and E. Cabib. 1966. Mannan synthetase from yeast. *Methods Enzymol.* 8:411–416.

Almonacid, M., and A. Paoletti. 2010. Mechanisms controlling division-plane positioning. *Semin. Cell Dev. Biol.* 21:874–880. http://dx.doi.org/10.1016/j.semcdb.2010.08.006

Balasubramanian, M.K., R. Srinivasan, Y. Huang, and K.H. Ng. 2012. Comparing contractile apparatus-driven cytokinesis mechanisms across kingdoms. *Cytoskeleton (Hoboken)*. 69:942–956. http://dx.doi.org/10.1002/cm.21082

Bathe, M., and F. Chang. 2010. Cytokinesis and the contractile ring in fission yeast: towards a systems-level understanding. *Trends Microbiol.* 18:38–45. http://dx.doi.org/10.1016/j.tim.2009.10.002

Cabib, E., D.H. Roh, M. Schmidt, L.B. Crotti, and A. Varma. 2001. The yeast cell wall and septum as paradigms of cell growth and morphogenesis. *J. Biol. Chem.* 276:19679–19682. http://dx.doi.org/10.1074/jbc.R000031200

Carnahan, R.H., and K.L. Gould. 2003. The PCH family protein, Cdc15p, recruits two F-actin nucleation pathways to coordinate cytokinetic actin ring formation in *Schizosaccharomyces pombe. J. Cell Biol.* 162:851–862. http://dx.doi.org/10.1083/jcb.200305012

Castro, C., J.C. Ribas, M.H. Valdivieso, R. Varona, F. del Rey, and A. Durán. 1995. Papulacandin B resistance in budding and fission yeasts: isolation and characterization of a gene involved in (1,3)β-D-glucan synthesis in *Saccharomyces cerevisiae. J. Bacteriol.* 177:5732–5739.

Chang, E.C., M. Barr, Y. Wang, V. Jung, H.P. Xu, and M.H. Wigler. 1994. Cooperative interaction of *S. pombe* proteins required for mating and morphogenesis. *Cell*. 79:131–141. http://dx.doi.org/10.1016/0092-8674(94)90406-5

Cortés, J.C.G., J. Ishiguro, A. Durán, and J.C. Ribas. 2002. Localization of the (1,3)β-D-glucan synthase catalytic subunit homologue Bgs1p/Cps1p from fission yeast suggests that it is involved in septation, polarized growth, mating, spore wall formation and spore germination. *J. Cell Sci.* 115:4081–4096. http://dx.doi.org/10.1242/jcs.00085

Cortés, J.C.G., E. Carnero, J. Ishiguro, Y. Sánchez, A. Durán, and J.C. Ribas. 2005. The novel fission yeast (1,3)β-D-glucan synthase catalytic subunit Bgs4p is essential during both cytokinesis and polarized growth. *J. Cell Sci.* 118:157–174. http://dx.doi.org/10.1242/jcs.01585

Cortés, J.C.G., M. Konomi, I.M. Martins, J. Muñoz, M.B. Moreno, M. Osumi, A. Durán, and J.C. Ribas. 2007. The (1,3)β-D-glucan synthase subunit Bgs1p is responsible for the fission yeast primary septum formation. *Mol. Microbiol*. 65:201–217. http://dx.doi.org/10.1111/j.1365-2958.2007.05784.x

Cortés, J.C.G., M. Sato, J. Muñoz, M.B. Moreno, J.A. Clemente-Ramos, M. Ramos, H. Okada, M. Osumi, A. Durán, and J.C. Ribas. 2012. Fission yeast Ags1 confers the essential septum strength needed for safe gradual cell abscission. *J. Cell Biol.* 198:637–656. http://dx.doi.org/10.1083/jcb.201202015

Egel, R. 1984. Two tightly linked silent cassettes in the mating-type region of *Schizosaccharomyces pombe. Curr. Genet.* 8:199–203. http://dx.doi.org/10.1007/BF00417816

Hartland, R.P., C.A. Vermeulen, F.M. Klis, J.H. Sietsma, and J.G. Wessels. 1994. The linkage of (1-3)-β-glucan to chitin during cell wall assembly in *Saccharomyces cerevisiae. Yeast*. 10:1591–1599. http://dx.doi.org/10.1002/yea.320101208

Hochstenbach, F., F.M. Klis, H. van den Ende, E. van Donselaar, P.J. Peters, and R.D. Klausner. 1998. Identification of a putative α-glucan synthase essential for cell wall construction and morphogenesis in fission yeast. *Proc. Natl. Acad. Sci. USA*. 95:9161–9166. http://dx.doi.org/10.1073/pnas.95.16.9161

Huang, Y., H. Yan, and M.K. Balasubramanian. 2008. Assembly of normal actomyosin rings in the absence of Mid1p and cortical nodes in fission yeast. *J. Cell Biol.* 183:979–988. http://dx.doi.org/10.1083/jcb.200806151

Humbel, B.M., M. Konomi, T. Takagi, N. Kamasawa, S.A. Ishijima, and M. Osumi. 2001. In situ localization of β-glucans in the cell wall of *Schizosaccharomyces pombe. Yeast*. 18:433–444. http://dx.doi.org/10.1002/yea.694

Hwang, H.Y., S.K. Olson, J.D. Esko, and H.R. Horvitz. 2003. *Caenorhabditis elegans* early embryogenesis and vulval morphogenesis require chondroitin biosynthesis. *Nature*. 423:439–443. http://dx.doi.org/10.1038/nature01634

Hynes, R.O., and A. Naba. 2012. Overview of the matrisome—an inventory of extracellular matrix constituents and functions. *Cold Spring Harb. Perspect. Biol*. 4:a004903. http://dx.doi.org/10.1101/cshperspect.a004903

Izumikawa, T., N. Kanagawa, Y. Watamoto, M. Okada, M. Saeki, M. Sakano, K. Sugahara, K. Sugihara, M. Asano, and H. Kitagawa. 2010. Impairment of embryonic cell division and glycosaminoglycan biosynthesis in glucuronyltransferase-I-deficient mice. *J. Biol. Chem.* 285:12190–12196. http://dx.doi.org/10.1074/jbc.M110.100941

Johnson, B.F., B.Y. Yoo, and G.B. Calleja. 1973. Cell division in yeasts: movement of organelles associated with cell plate growth of *Schizosaccharomyces pombe. J. Bacteriol.* 115:358–366.

Johnson, B.F., B.Y. Yoo, G.B. Calleja, and C.P. Kozela. 2005. Second thoughts on septation by the fission yeast, *Schizosaccharomyces pombe*: pull vs. push mechanisms with an appendix—dimensional modelling of the flat and variable septa. *Antonie van Leeuwenhoek*. 88:1–12. http://dx.doi.org/10.1007/s10482-004-7074-2

Jordan, S.N., S. Olson, and J.C. Canman. 2011. Cytokinesis: thinking outside the cell. *Curr. Biol.* 21:R119–R121. http://dx.doi.org/10.1016/j.cub.2010.12.040

Katayama, S., D. Hirata, M. Arellano, P. Pérez, and T. Toda. 1999. Fission yeast α-glucan synthase Mok1 requires the actin cytoskeleton to localize the sites of growth and plays an essential role in cell morphogenesis downstream of protein kinase C function. *J. Cell Biol.* 144:1173–1186. http://dx.doi.org/10.1083/jcb.144.6.1173

Konomi, M., K. Fujimoto, T. Toda, and M. Osumi. 2003. Characterization and behaviour of α-glucan synthase in *Schizosaccharomyces pombe* as revealed by electron microscopy. *Yeast*. 20:427–438. http://dx.doi.org/10.1002/yea.974

Lee, I.J., V.C. Coffman, and J.Q. Wu. 2012. Contractile-ring assembly in fission yeast cytokinesis: Recent advances and new perspectives. *Cytoskeleton (Hoboken)*. 69:751–763. http://dx.doi.org/10.1002/cm.21052

Liu, J., X. Tang, H. Wang, S. Oliferenko, and M.K. Balasubramanian. 2002. The localization of the integral membrane protein Cps1p to the cell division site is dependent on the actomyosin ring and the septation-inducing network in *Schizosaccharomyces pombe. Mol. Biol. Cell*. 13:989–1000. http://dx.doi.org/10.1091/mbc.01-12-0581

Liu, J., G.D. Fairn, D.F. Ceccarelli, F. Sicheri, and A. Wilde. 2012. Cleavage furrow organization requires PIP(2)-mediated recruitment of anillin. *Curr. Biol.* 22:64–69. http://dx.doi.org/10.1016/j.cub.2011.11.040

Lu, P., V.M. Weaver, and Z. Werb. 2012. The extracellular matrix: a dynamic niche in cancer progression. *J. Cell Biol.* 196:395–406. http://dx.doi.org/10.1083/jcb.201102147

Maeda, Y., J. Kashiwazaki, C. Shimoda, and T. Nakamura. 2009. The *Schizosaccharomyces pombe* syntaxin 1 homolog, Psy1, is essential in the development of the forespore membrane. *Biosci. Biotechnol. Biochem.* 73:339–345. http://dx.doi.org/10.1271/bbb.80575

Martín, V., B. García, E. Carnero, A. Durán, and Y. Sánchez. 2003. Bgs3p, a putative 1,3-β-glucan synthase subunit, is required for cell wall assembly in *Schizosaccharomyces pombe. Eukaryot. Cell*. 2:159–169. http://dx.doi.org/10.1128/EC.2.1.159-169.2003

Martins, I.M., J.C.G. Cortés, J. Muñoz, M.B. Moreno, M. Ramos, J.A. Clemente-Ramos, A. Durán, and J.C. Ribas. 2011. Differential activities of three families of specific β(1,3)glucan synthase inhibitors in wild-type and resistant strains of fission yeast. *J. Biol. Chem.* 286:3484–3496. http://dx.doi.org/10.1074/jbc.M110.174300

Mishra, M., Y. Huang, P. Srivastava, R. Srinivasan, M. Sevugan, R. Shlomovitz, N. Gov, M. Rao, and M. Balasubramanian. 2012. Cylindrical cellular geometry ensures fidelity of division site placement in fission yeast. *J. Cell Sci.* 125:3850–3857. http://dx.doi.org/10.1242/jcs.103788

Mizuguchi, S., T. Uyama, H. Kitagawa, K.H. Nomura, K. Dejima, K. Gengyo-Ando, S. Mitani, K. Sugahara, and K. Nomura. 2003. Chondroitin proteoglycans are involved in cell division of *Caenorhabditis elegans. Nature*. 423:443–448. http://dx.doi.org/10.1038/nature01635

Moreno, S., A. Klar, and P. Nurse. 1991. Molecular genetic analysis of fission yeast *Schizosaccharomyces pombe. Methods Enzymol.* 194:795–823. http://dx.doi.org/10.1016/0076-6879(91)94059-L

Moreno, M.B., A. Durán, and J.C. Ribas. 2000. A family of multifunctional thiamine-repressible expression vectors for fission yeast. *Yeast*. 16:861–872. http://dx.doi.org/10.1002/1097-0061(20000630)16:9<861::AID-YEA577>3.0.CO;2-9

Naqvi, N.I., K. Eng, K.L. Gould, and M.K. Balasubramanian. 1999. Evidence for F-actin-dependent and -independent mechanisms involved in assembly and stability of the medial actomyosin ring in fission yeast. *EMBO J.* 18:854–862. http://dx.doi.org/10.1093/emboj/18.4.854

Naqvi, N.I., K.C. Wong, X. Tang, and M.K. Balasubramanian. 2000. Type II myosin regulatory light chain relieves auto-inhibition of myosin-heavy-chain function. *Nat. Cell Biol.* 2:855–858. http://dx.doi.org/10.1038/35041107

Olson, S.K., J.R. Bishop, J.R. Yates, K. Oegema, and J.D. Esko. 2006. Identification of novel chondroitin proteoglycans in *Caenorhabditis elegans*: embryonic cell division depends on CPG-1 and CPG-2. *J. Cell Biol.* 173:985–994. http://dx.doi.org/10.1083/jcb.200603003

Osumi, M., N. Yamada, H. Kobori, A. Taki, N. Naito, M. Baba, and T. Nagatani. 1989. Cell wall formation in regenerating protoplasts of *Schizosaccharomyces pombe*: study by high resolution, low voltage scanning electron microscopy. *J. Electron Microsc. (Tokyo)*. 38:457–468.

Pardo, M., and P. Nurse. 2003. Equatorial retention of the contractile actin ring by microtubules during cytokinesis. *Science*. 300:1569–1574. http://dx.doi.org/10.1126/science.1084671

Pérez, P., and J. Cansado. 2010. Cell integrity signaling and response to stress in fission yeast. *Curr. Protein Pept. Sci.* 11:680–692. http://dx.doi.org/10.2174/138920310794557718

Pérez, P., and J.C. Ribas. 2004. Cell wall analysis. *Methods*. 33:245–251. http://dx.doi.org/10.1016/j.ymeth.2003.11.020

Perez, P., and S.A. Rincón. 2010. Rho GTPases: regulation of cell polarity and growth in yeasts. *Biochem. J.* 426:243–253. http://dx.doi.org/10.1042/BJ20091823

Pollard, T.D. 2010. Mechanics of cytokinesis in eukaryotes. *Curr. Opin. Cell Biol.* 22:50–56. http://dx.doi.org/10.1016/j.ceb.2009.11.010

Proctor, S.A., N. Minc, A. Boudaoud, and F. Chang. 2012. Contributions of turgor pressure, the contractile ring, and septum assembly to forces in cytokinesis in fission yeast. *Curr. Biol.* 22:1601–1608. http://dx.doi.org/10.1016/j.cub.2012.06.042

Ribas, J.C., M. Díaz, A. Durán, and P. Pérez. 1991. Isolation and characterization of *Schizosaccharomyces pombe* mutants defective in cell wall (1-3)β-D-glucan. *J. Bacteriol.* 173:3456–3462.

Rincón, S.A., and A. Paoletti. 2012. Mid1/anillin and the spatial regulation of cytokinesis in fission yeast. *Cytoskeleton (Hoboken)*. 69:764–777. http://dx.doi.org/10.1002/cm.21056

Roncero, C., and Y. Sánchez. 2010. Cell separation and the maintenance of cell integrity during cytokinesis in yeast: the assembly of a septum. *Yeast*. 27:521–530. http://dx.doi.org/10.1002/yea.1779

Sambrook, J., and D.W. Russell. 2001. Molecular cloning: a laboratory manual. Cold Spring Harbor Laboratory Press, Cold Spring Harbor, NY. 2344 pp.

Shaner, N.C., P.A. Steinbach, and R.Y. Tsien. 2005. A guide to choosing fluorescent proteins. *Nat. Methods*. 2:905–909. http://dx.doi.org/10.1038/nmeth819

Sipiczki, M. 2007. Splitting of the fission yeast septum. *FEMS Yeast Res.* 7:761–770. http://dx.doi.org/10.1111/j.1567-1364.2007.00266.x

Sipiczki, M., M. Yamaguchi, A. Grallert, K. Takeo, E. Zilahi, A. Bozsik, and I. Miklos. 2000. Role of cell shape in determination of the division plane in *Schizosaccharomyces pombe*: random orientation of septa in spherical cells. *J. Bacteriol.* 182:1693–1701. http://dx.doi.org/10.1128/JB.182.6.1693-1701.2000

Verde, F., J. Mata, and P. Nurse. 1995. Fission yeast cell morphogenesis: identification of new genes and analysis of their role during the cell cycle. *J. Cell Biol.* 131:1529–1538. http://dx.doi.org/10.1083/jcb.131.6.1529

White, J., and S. Bednarek. 2003. Cytokinesis: GAGs form the walls that separate our parts. *Curr. Biol.* 13:R717–R718. http://dx.doi.org/10.1016/j.cub.2003.08.048

Wu, J.Q., J.R. Kuhn, D.R. Kovar, and T.D. Pollard. 2003. Spatial and temporal pathway for assembly and constriction of the contractile ring in fission yeast cytokinesis. *Dev. Cell*. 5:723–734. http://dx.doi.org/10.1016/S1534-5807(03)00324-1

Xu, X., and B.E. Vogel. 2011. A secreted protein promotes cleavage furrow maturation during cytokinesis. *Curr. Biol.* 21:114–119. http://dx.doi.org/10.1016/j.cub.2010.12.006

Zhang, X., A.V. Bedigian, W. Wang, and U.S. Eggert. 2012. G protein-coupled receptors participate in cytokinesis. *Cytoskeleton (Hoboken)*. 69:810–818. http://dx.doi.org/10.1002/cm.21055

Muñoz et al., http://www.jcb.org/cgi/content/full/jcb.201304132/DC1

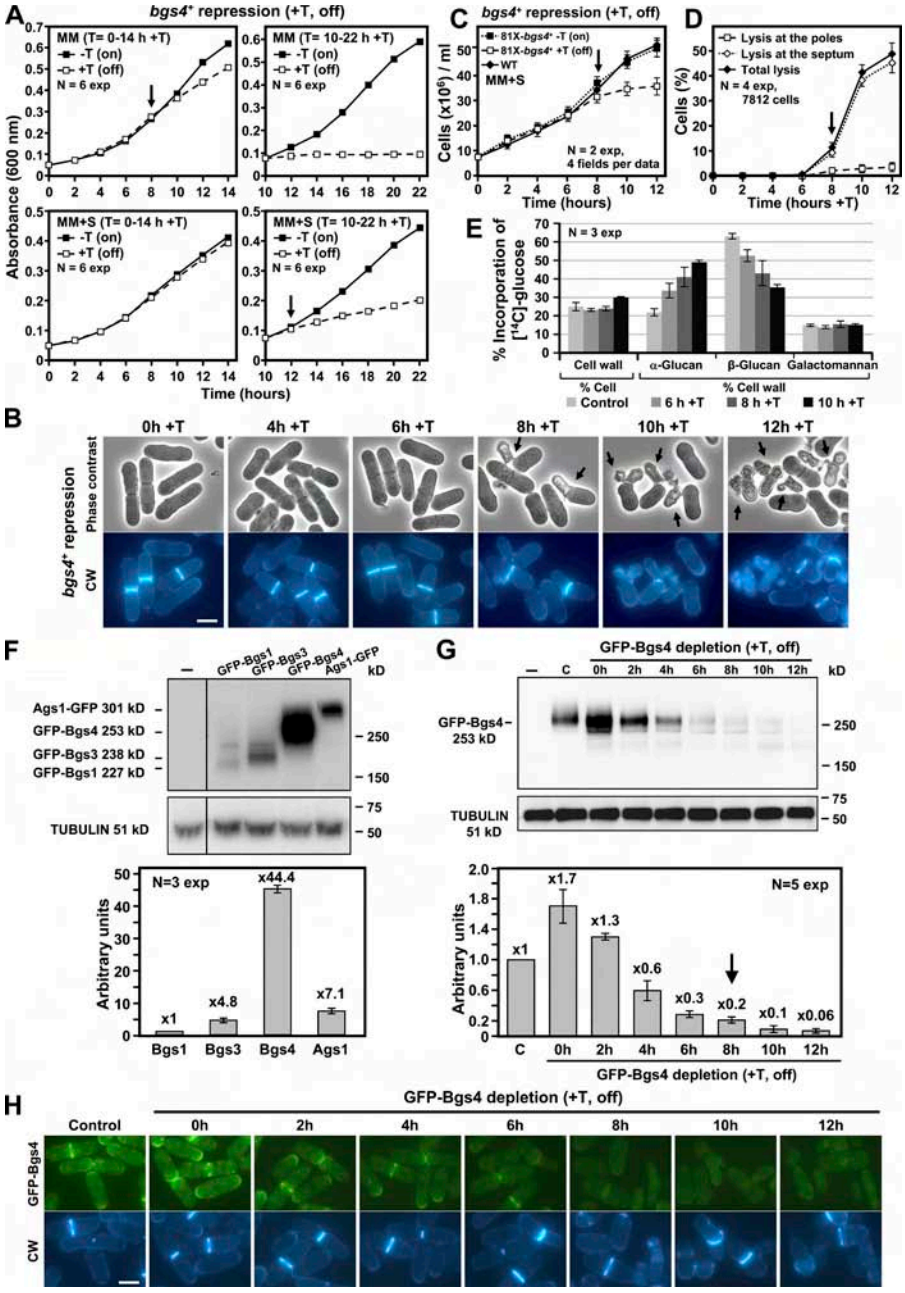

Figure S1. **Absence of Bgs4 promotes cell lysis and cytoplasm release during both cytokinesis and polarized growth.** (A) Sorbitol partially suppresses the cell growth arrest (arrow) promoted by *bgs4*$^+$ repression. 81X-*bgs4*$^+$ cells were grown in MM either without or with thiamine (−T, induced; +T, repressed) and 1.2 M sorbitol (S). Cell growth was monitored at the indicated times (n = 2), from 0 to 14 h and from 10 to 22 h. Cell growth arrest was more apparent from 10 to 22 h, probably because of the diluted cell density and the differences in cell wall composition between early and late log-phase cells, in which the cell wall may change to a more rigid cell wall of stationary phase cells (not depicted). The data shown are from a single representative experiment out of six repeats (two different 81X-*bgs4*$^+$ strains analyzed in three independent experiments). (B) The absence of Bgs4 promotes cell lysis (arrows) before cell growth arrest is detected. Cells were grown in MM+S+T as in A and visualized. A similar cell lysis earlier than cell growth arrest, at 5–6 h of *bgs4*$^+$ repression, was also observed in the absence of sorbitol (not depicted). (C) Bgs4 absence causes an arrest in the increase in cell number (arrow) coincident with the start of cell lysis observed in B. The discrepancy between absorbance and cell number arrests could be caused by an additional absorbance of lysed cells, released cytoplasmic material, or changes in cell shape, volume, density, cell wall thickness, or cell wall composition. Cells were grown as in B and the cell number was monitored at the indicated times (n = 2; four fields per data). (D) Absence of Bgs4 promotes cell lysis (arrow) mainly at the septum and some at the poles. Cells were grown as in B. (E) Bgs4 depletion causes a progressive decrease in cell wall total β-glucan (B-BG, L-BG, and β(1,6)glucan) and a concomitant increase in cell wall α-glucan. Cells were grown as in B, maintained in the early log-phase by the corresponding dilution of the cell culture, and collected at the indicated times. [^{14}C]Glucose was added 4 h before harvesting in each case. Incorporation of [^{14}C]glucose into cell wall polysaccharides was analyzed as indicated (see Materials and methods). (F and G) Bgs4 is the most abundant GS (F; native promoters) and decreases drastically during *bgs4*$^+$ repression (G; *nmt1*$^+$-81X repressible promoter). Proteins from total cell extracts (80 µg) were separated in 3–8% SDS-PAGE, blotted, and probed with monoclonal anti-GFP or anti–α-tubulin antibody. Relative amounts of protein were quantified in comparison with tubulin. (G) Lane –, control without GFP tag; lane C, control of Bgs4 expressed from its native promoter; arrow, cell lysis start. Black lines in F indicate the removal of intervening lanes for presentation purposes. (H) GFP-Bgs4 localization is undetectable after 8 h of *bgs4*$^+$ repression. Cells were grown as in B and imaged. The number of experiments and total cells analyzed is shown in each case. Bars, 5 µm.

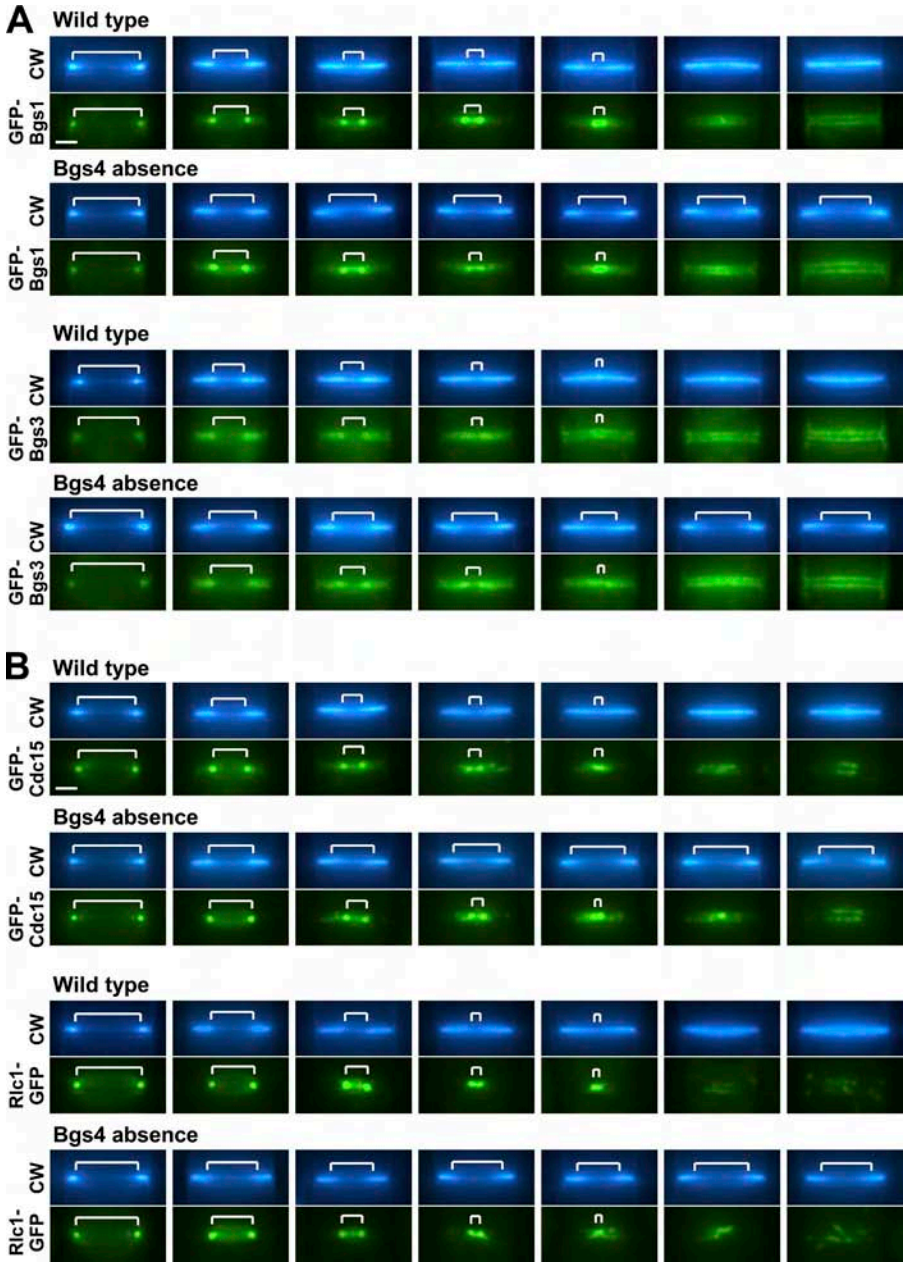

Figure S2. **Bgs4 is required for CW-stained PS completion but not for CAR contraction and septum PM closure.** (A) The defect in CW-stained open PS does not correspond to a general defect in septum formation. The progression (brackets) of CW-stained PS is coincident with that of WT septum membrane proteins (Bgs1 and Bgs3), but not in the absence of Bgs4. (B) The defect in CW-stained open PS does not correspond to a general defect in CAR contraction. The progression (brackets) of CW-stained PS is coincident with that of WT CAR proteins (Cdc15 and Rlc1) but not in the absence of Bgs4. Early log-phase WT and 81X-*bgs4*$^{+}$ cells expressing *GFP-bgs1*$^{+}$, *GFP-bgs3*$^{+}$, *GFP-cdc15*$^{+}$, or *rlc1*$^{+}$*-GFP* were grown in MM+S+T for 10 h at 30°C and visualized. Bars, 1 µm.

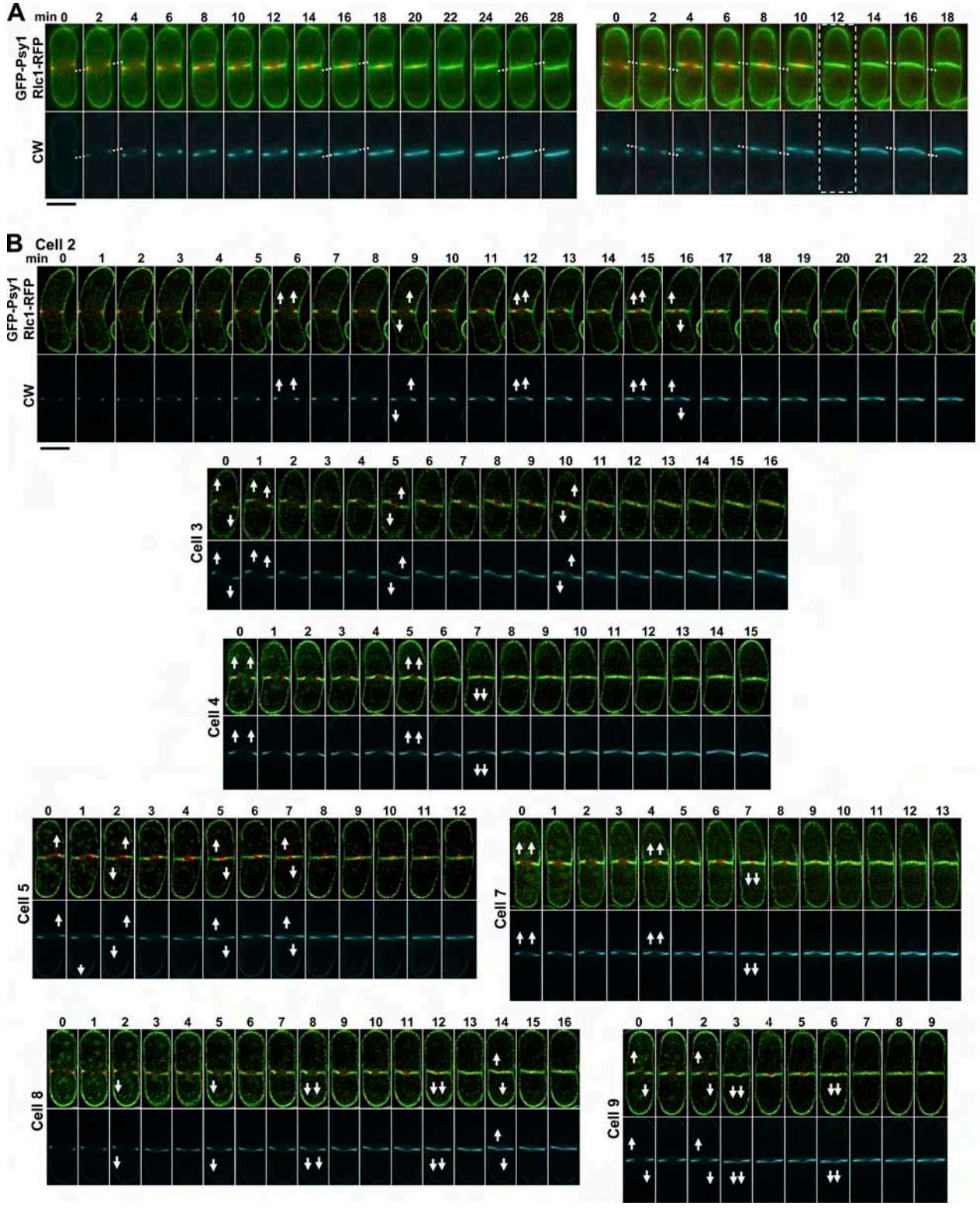

Figure S3. **Bgs4 and its β(1,3)glucan are required for correct and stable CAR positioning in the cell middle and for correct straight CAR constriction and septum ingression.** (A) The defect in Bgs4 function (shown in the *cwg1-2* mutant allele) causes oblique positioning and ingression of CAR and septa (dotted line) similar to those observed in the absence of Bgs4. During CAR and septum ingression, the CAR (Rlc1-RFP) remains attached to the septum membrane (GFP-Psy1), whereas the CW-stained septum formation is uncoupled and delayed (dashed rectangle). (B) The defect in Bgs4 function (shown in the *cwg1-1* mutant allele) produces misdirected CAR contraction and septum progression (arrows) similar to those observed in the absence of Bgs4. During misdirected CAR contraction and septum ingression, the CAR (Rlc1-RFP) stays attached to the septum membrane (GFP-Psy1) and the CW-stained septum formation is delayed. CW staining shows the details of wavy septa, indicative of relaxed CAR with multiple changes in the direction of septum synthesis. Early log-phase *cwg1-2 GFP-psy1⁺ rlc1⁺-RFP* (A) and *cwg1-1 GFP-psy1⁺ rlc1⁺-RFP* (B) cells grown in YES medium at 25°C were shifted to 37°C for 5–6 h and visualized by time-lapse CW staining (5 µg/ml) and GFP and RFP fluorescence microscopy. Elapsed time is shown in minutes. Bars, 5 µm.

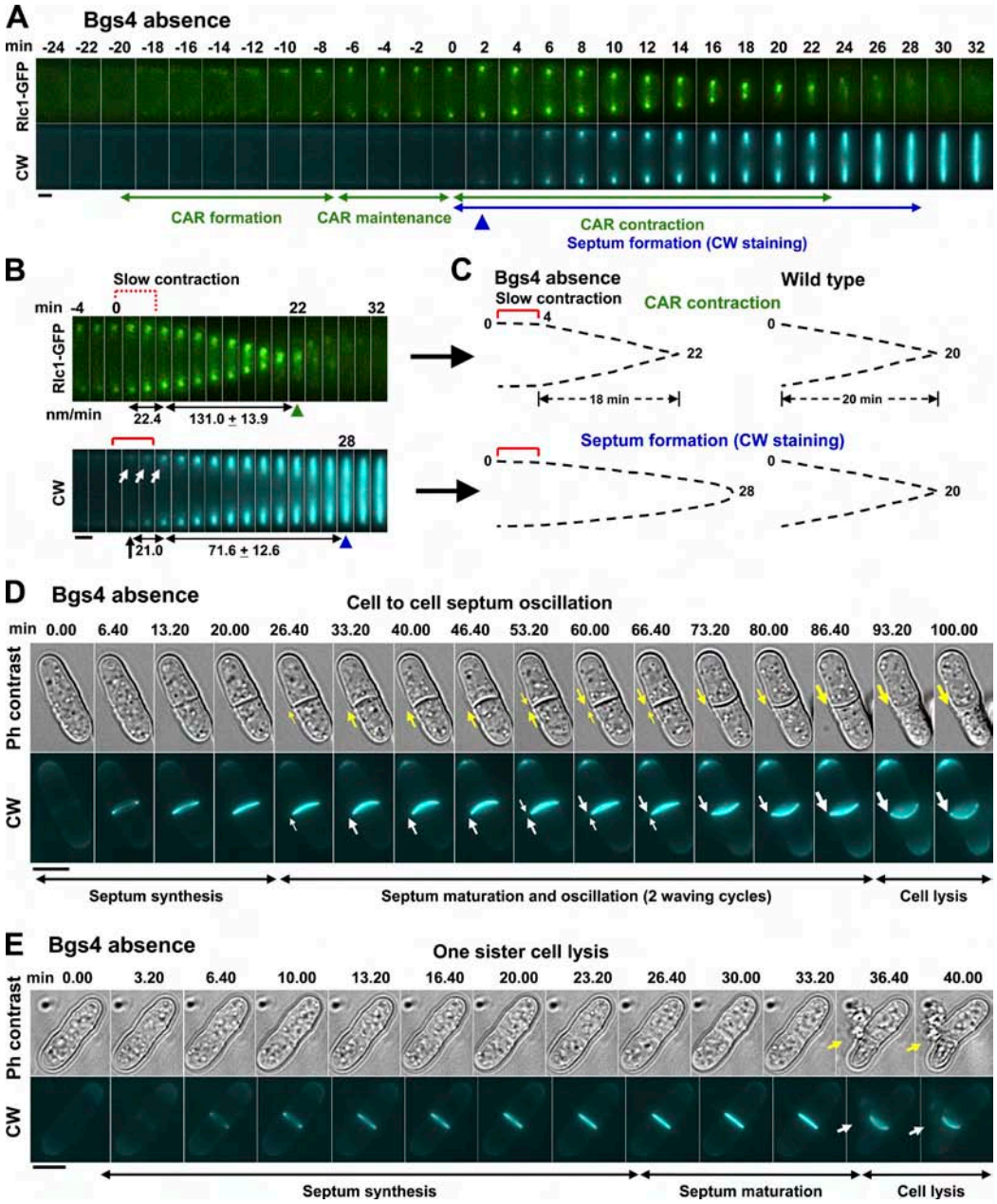

Figure S4. **Bgs4 is essential for coupling septum formation to CAR contraction.** After septum completion, Bgs4 is also required to confer the septum rigidity necessary to withstand the internal turgor pressure and to protect the cell integrity at the start of cell separation. (A–C) Bgs4 absence originates an uncoupling between CAR contraction and the slower CW-stained septum formation. (A) Early log-phase WT *rlc1*$^{+}$*-GFP* and 81X-*bgs4*$^{+}$ *rlc1*$^{+}$*-GFP* cells were grown in MM+S+T for 8 h at 30°C and visualized by time-lapse CW staining (5 µg/ml) and GFP fluorescence microscopy. Green double arrow, time interval of CAR formation, CAR maintenance, and CAR contraction; blue double arrow, time interval of septum formation; blue arrowhead, first image where the CW-stained septum is detected (t = 2), considering the previous image as the start (t = 0) of septum synthesis. Elapsed time is shown in minutes. (B) Bgs4 absence originates a defective initial slow CAR contraction and a constantly slower septum synthesis, uncoupling CAR contraction from septum formation. Kymographs of the CAR contraction and CW-stained septum formation observed in A. Black arrow (t = 2), first image where the CW-stained septum is detected; arrowhead, end of CAR contraction (green; t = 22) and septum formation (blue; t = 28); red bracket, interval (first 4–6 min) of defective initial slow CAR contraction (dotted line) and septum formation (solid line); white arrows, asymmetric septum synthesis coincident with defective slow CAR contraction. Elapsed time is shown in minutes. The rates of CAR contraction and septum formation (intervals 2–6, 6–12, and 12–18 min) were calculated and are shown in nanometers per minute. The 6–18-min interval shows the mean of the 6–12- and 12–18-min intervals. (C) Scheme of CAR contraction and septum formation in the kymographs of the Bgs4-depleted cell shown in B and a WT cell (see Fig. 4, C and D). Bgs4 absence originates a defective initial slow CAR contraction and septum formation (red brackets). The rest of CAR contraction proceeds even faster than that of WT cells. However, the defect in septum formation continues, increasing the time required for septum completion. Numbers indicate the time needed for completion of CAR contraction and septum formation in each case. (D) In the absence of Bgs4 the septum becomes flexible and curved, swinging according to the changes in internal turgor pressure in the sister cells. Small and large arrows represent the gradual increase in internal turgor pressure in the corresponding cell, promoting the curvature of the septum. Then, the opposite cell reacts and increases its internal pressure above that of the sister cell, originating septum oscillation. Two waving cycles until cell lysis appears are shown (see also Fig. 5, C and D). (E) After septum synthesis and maturation, the absence of Bgs4 promotes cell lysis and the release of cytoplasmic material (arrow) from the division site when cell separation begins, resulting in the death of either one or both sister cells (see also Fig. 7 D). Early log-phase 81X-*bgs4*$^{+}$ cells were grown in MM+S+T for 9 (D) or 10 (E) h at 30°C and visualized by time-lapse phase-contrast and CW staining (5 µg/ml) microscopy. Elapsed time is shown in minutes. Bars: (cells) 5 µm; (septum details) 1 µm.

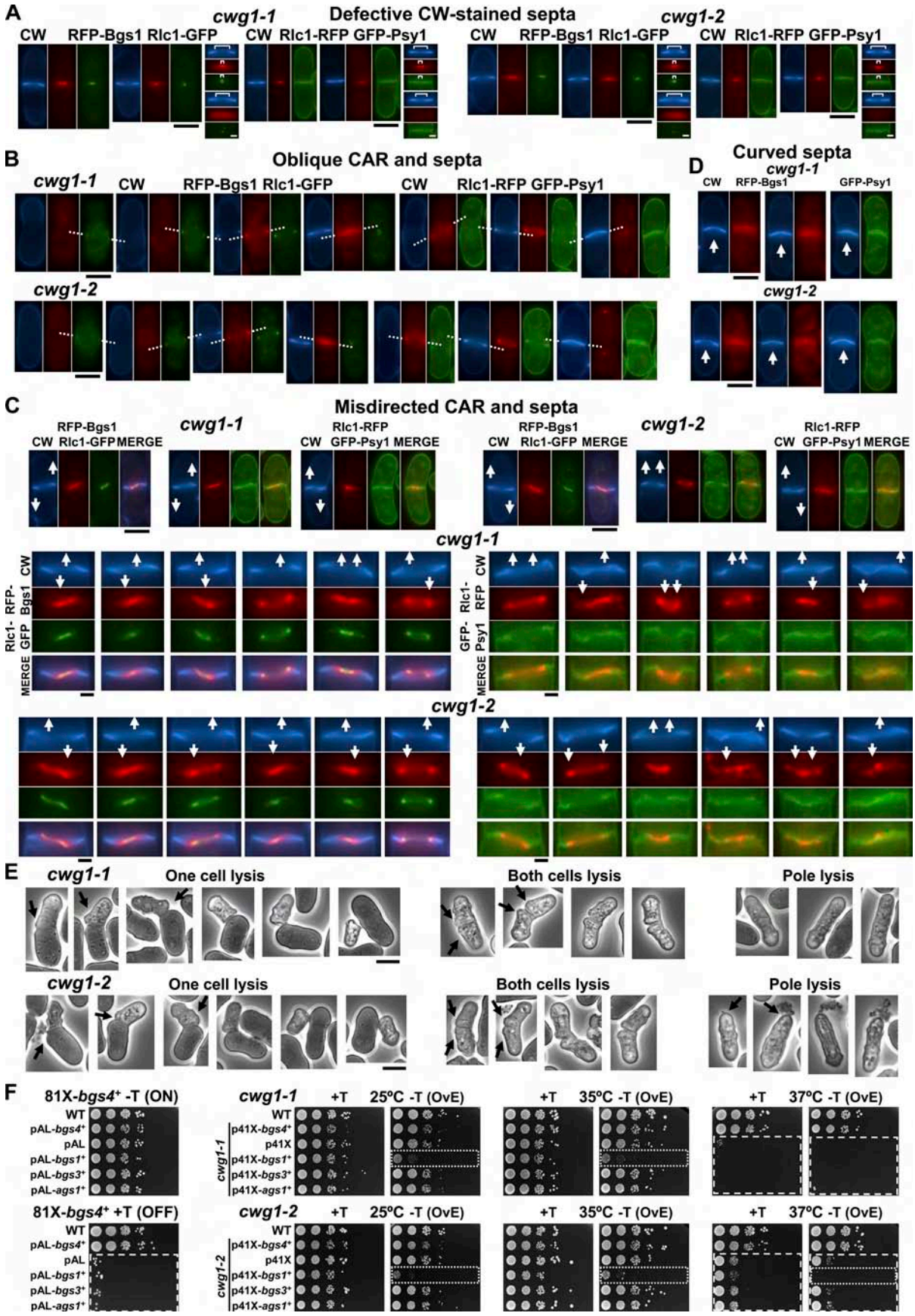
A
cwg1-1
Defective CW-stained septa
cwg1-2
CW RFP-Bgs1 Rlc1-GFP
CW Rlc1-RFP GFP-Psy1
B
Oblique CAR and septa
cwg1-1
cwg1-2
D
Curved septa
C
Misdirected CAR and septa
RFP-Bgs1
Rlc1-GFP
MERGE
Rlc1-RFP
GFP-Psy1
E
One cell lysis
Both cells lysis
Pole lysis
F
81X-bgs4+ -T (ON)
81X-bgs4+ +T (OFF)
WT
pAL-bgs4+
pAL
pAL-bgs1+
pAL-bgs3+
pAL-ags1+
+T 25ºC -T (OvE)
+T 35ºC -T (OvE)
+T 37ºC -T (OvE)
p41X-bgs4+
p41X
p41X-bgs1+
p41X-bgs3+
p41X-ags1+

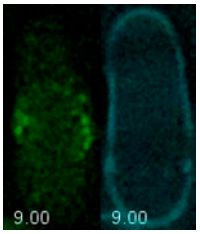

Video 1. **Formation of an oblique CAR and septum of two dividing Bgs4-depleted cells.** 81X-*bgs4*$^{+}$ *rlc1*$^{+}$*-GFP* cells were grown in the presence of thiamine and 1.2 M sorbitol for 10 h at 28°C and imaged by time-lapse Rlc1-GFP and CW staining (5 µg/ml) fluorescence microscopy, using an inverted microscope (IX71; Olympus) equipped with a Personal DeltaVision system (Applied Precision). Cells were observed for 180 min. Frames of selected cells were taken every 3 min. To decrease the movie length, the frames only show the stages of CAR formation and the beginning of CAR contraction and septum formation (t = 39 min). Videos 3, 4 (cells 3 and 4, right), 8, 9, and 10 (cells 1 and 2) also show the formation of oblique CAR and septa.

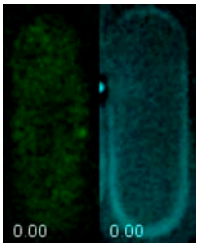

Video 2. **Formation of an altered CAR but normal septum of two dividing Bgs4-depleted cells.** An oblique CAR slides to a perpendicular position and a perpendicular CAR slides along the PM before the start of perpendicular septation. 81X-*bgs4*$^{+}$ *rlc1*$^{+}$*-GFP* cells were grown in the presence of thiamine and 1.2 M sorbitol for 10 h at 28°C and imaged by time-lapse Rlc1-GFP and CW staining (5 µg/ml) fluorescence microscopy, using an inverted microscope (IX71; Olympus) equipped with a Personal DeltaVision system (Applied Precision). Cells were observed for 180 min. Frames of selected cells were taken every 3 min. To decrease the movie length, the frames only show the stages of CAR formation and the beginning of CAR contraction and septum formation (t = 33 and 42 min).

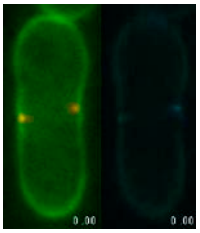

Video 3. **Formation of an oblique CAR and septum of four *S. pombe* cells expressing the *cwg1-2* thermosensitive mutant allele of *bgs4*$^{+}$.** During CAR and septum ingression, the CAR (Rlc1-RFP) remains attached to the septum membrane (GFP-Psy1), whereas the CW-stained septum formation is uncoupled and delayed. Early log-phase *cwg1-2 GFP-psy1*$^{+}$ *rlc1*$^{+}$*-RFP* cells grown in YES medium at 25°C were shifted to 37°C for 5–6 h and imaged by time-lapse GFP-Psy1, Rlc1-RFP, and CW staining (5 µg/ml) fluorescence microscopy, using an inverted microscope (IX71; Olympus) equipped with a Personal DeltaVision system (Applied Precision). Cells were observed for 120 min. Frames of selected cells were taken every 2 min. To decrease the movie length, the frames only show the stages of CAR positioning and contraction and septum formation (t = 24, 26, and 28 min).

Figure S5. **The Bgs4-defective *cwg1-1* and *cwg1-2* thermosensitive mutants show the same cytokinesis and cell integrity defects as those observed in the absence of Bgs4.** The defects in septum synthesis and cell integrity promoted by the absence of or defective Bgs4 function cannot be compensated by the function of any other GS. (A–D) The Bgs4-defective *cwg1-1* and *cwg1-2* mutants present (A) defective CW-stained open septa (bracket) in septa with advanced and complete CAR (Rlc1-GFP and Rlc1-RFP) and septum membranes (RFP-Bgs1 and GFP-Psy1). (B) Oblique positioning and ingression (dotted line) of nodes, CAR (Rlc1-GFP and Rlc1-RFP), septum membranes (RFP-Bgs1 and GFP-Psy1), and septum walls (CW staining). (C) Misdirected (arrows) CAR contraction (Rlc1-GFP and Rlc1-RFP) and septum membrane and wall progression (RFP-Bgs1, GFP-Psy1, and CW-staining), observed in cells and in magnified septa showing the details of CW-stained wavy septa, indicative of relaxed CAR with multiple changes in the direction of septum synthesis. (D) Curved (arrow) complete septa (RFP-Bgs1 and GFP-Psy1) caused by the differences in internal turgor pressure between sister cells. In all cases, during CAR and septum ingression the CAR (Rlc1-GFP and Rlc1-RFP) stays attached to the septum membrane (RFP-Bgs1 and GFP-Psy1), whereas in many of these cells the CW-stained septum formation is uncoupled and delayed. Early log-phase Bgs4-defective *cwg1-1* and *cwg1-2* mutants expressing either *RFP-bgs1*$^{+}$ *rlc1*$^{+}$*-GFP* or *GFP-psy1*$^{+}$ *rlc1*$^{+}$*-RFP* and grown in YES medium at 25°C were shifted to 37°C for 5–7 h and examined by CW staining (50 µg/ml) and GFP and RFP fluorescence microscopy. (E) The Bgs4-defective *cwg1-1* and *cwg1-2* mutants are also involved in cell integrity maintenance. Both mutant alleles promote major cell lysis after septum maturation from either one (left) or both (middle) sister cells, and a minor cell lysis and cytoplasm release from the poles (right). Early log-phase *cwg1-1* and *cwg1-2* mutant cells were grown as in A–D and visualized by phase-contrast microscopy. Although all the Bgs4 absence phenotypes are present in both *cwg1-1* and *cwg1-2* mutants, the amount of each type of defect differs between the *cwg1-1* and *cwg1-2* mutant alleles. Misdirected CAR and septa are much more abundant and aggravated in *cwg1-1* cells, whereas oblique CAR and septa and cell lysis defects, especially the pole lysis, are more abundant in *cwg1-2* cells (not depicted). (F) The increase in the function of any other GS (Ags1, Bgs1, and Bgs3) is unable to suppress the cytokinesis and cell integrity defects promoted by Bgs4 absence or Bgs4-defective *cwg1-1* or *cwg1-2* mutations. 81X-*bgs4*$^{+}$ strains transformed with multicopy pAL plasmid, either empty (negative control) or expressing *ags1*$^{+}$, *bgs1*$^{+}$, *bgs3*$^{+}$, or *bgs4*$^{+}$ (positive control) from their native promoters, were analyzed on MM-T (81X-*bgs4*$^{+}$ induced) and MM+T (81X-*bgs4*$^{+}$ repressed) plates at 28°C. The *cwg1-1* and *cwg1-2* thermosensitive mutants transformed with the overexpression plasmid p41X, either empty (negative control) or expressing *ags1*$^{+}$, *bgs1*$^{+}$, *bgs3*$^{+}$, or *bgs4*$^{+}$ (positive control) from the *nmt1*$^{+}$-41X promoter, were analyzed on MM+T (41X lower expression) and MM-T (41X overexpression; OvE) plates at 25, 28, 32, 35, and 37°C. In all cases, a WT strain was used as control. Early log-phase cells were adjusted to 10^{7} cells/ml, 1:10 serial diluted, spotted onto MM-T and MM+T plates, and incubated at the indicated temperatures for 3–4 d. The data shown are from a single representative experiment out of two repeats. The plates displaying differences in growth are shown. All the Bgs4-depleted or -defective *cwg1-1* or *cwg1-2* strains show the same cell lysis and growth arrest as those of the negative control strain (dashed rectangle). In addition, Bgs1 overproduction is deleterious when Bgs4 function is compromised, promoting in both *cwg1-1* and *cwg1-2* mutants a constitutive lytic defect at any temperature (dotted rectangle). Similarly, other defects in cytokinesis caused byBgs4 absence or Bgs4-defective *cwg1-1* or *cwg1-2* mutations are not suppressed by the overexpression of any other GS (not depicted). Bars: (cells) 5 µm; (septum details) 1 µm.

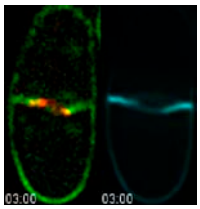

Video 4. **Formation of a misdirected CAR and septum of a *S. pombe* cell and magnification of the region of the division site during the formation of a misdirected CAR and septum of four cells expressing the *cwg1-1* thermosensitive mutant allele of *bgs4*$^{+}$.** During misdirected CAR contraction and septum ingression, the CAR (Rlc1-RFP) remains attached to the septum membrane (GFP-Psy1). CW staining shows the details of wavy septa, indicative of relaxed CAR with multiple changes in the direction of septum synthesis. Early log-phase *cwg1-1 GFP-psy1*$^{+}$ *rlc1*$^{+}$*-RFP* cells grown in YES medium at 25°C were shifted to 37°C for 5 h and imaged by time-lapse GFP-Psy1, Rlc1-RFP, and CW staining (5 μg/ml) fluorescence microscopy, using an inverted microscope (IX71; Olympus) equipped with a Personal DeltaVision system (Applied Precision). Cells were observed for 120 min. Frames of selected cells were taken every 60 s. To decrease the movie length, the frames only show the stages of CAR contraction and septum formation (cell, t = 17 min; septum details, t = 12, 15, 16, and 28 min).

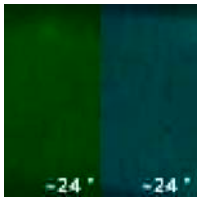

Video 5. **Coordinated CAR contraction and septum formation of a *S. pombe* WT cell.** WT *rlc1*$^{+}$*-GFP* cells were grown in the presence of thiamine and 1.2 M sorbitol for 8 h at 30°C and imaged by time-lapse Rlc1-GFP and CW staining (5 μg/ml) fluorescence microscopy, using an inverted microscope (IX71; Olympus) equipped with a Personal DeltaVision system (Applied Precision). Cells were observed for 180 min. Frames of selected cells were taken every 2 min. A magnification of the region of the division site is shown. To decrease the movie length, the frames only show the stages of CAR formation and contraction and septum formation from min −24 to 26. The start of septum synthesis (t = 0) was considered as the image before the first one where the CW-stained septum was detected (t = 2).

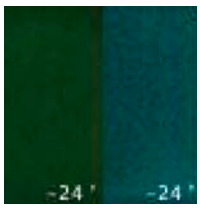

Video 6. **Uncoupling between CAR contraction and slower septum formation of three *S. pombe* Bgs4-depleted cells.** 81X-*bgs4*$^{+}$ *rlc1*$^{+}$*-GFP* cells were grown in the presence of thiamine and 1.2 M sorbitol for 8 h at 30°C and imaged by time-lapse Rlc1-GFP and CW staining (5 μg/ml) fluorescence microscopy, using an inverted microscope (IX71; Olympus) equipped with a Personal DeltaVision system (Applied Precision). Cells were observed for 180 min. Frames of selected cells were taken every 2 min. A magnification of the region of the division site is shown. To decrease the movie length, the frames only show the stages of CAR formation and contraction and septum formation from min −24 to 32. The start of septum synthesis (t = 0) was considered as the image before the first one where the CW-stained septum was detected (t = 2).

Video 7. **Formation of a rigid and straight septum and progressive cell separation of two dividing *S. pombe* WT cells.** WT cells were grown in the presence of thiamine and 1.2 M sorbitol for 9 h at 30°C and imaged by time-lapse phase-contrast and CW staining (5 μg/ml) microscopy, using an inverted microscope (IX71; Olympus) equipped with a Personal DeltaVision system (Applied Precision). Cells were observed for 180 min. Frames of selected cells were taken every 20 s. To decrease the movie length, the frames only show the stages of septum formation and cell separation (t = 37 min).

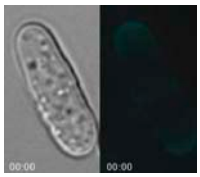

Video 8. **Formation of a flexible and oscillating curved septum with two waving cycles caused by the alternating changes in internal turgor pressure in the sister cells and ending with cell lysis of three dividing Bgs4-depleted cells.** 81X-*bgs4*$^{+}$ cells were grown in the presence of thiamine and 1.2 M sorbitol for 9 h at 30°C and imaged by time-lapse phase-contrast and CW staining (5 μg/ml) microscopy, using an inverted microscope (IX71; Olympus) equipped with a Personal DeltaVision system (Applied Precision). Cells were observed for 180 min. Frames of selected cells were taken every 20 s. To decrease the movie length, the frames only show the stages of septum formation, septum swinging with two waving cycles, and cell lysis (t = 87, 100 and, 117 min).

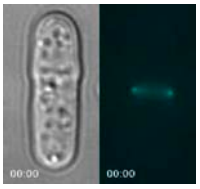

Video 9. **Formation of a flexible and oscillating curved septum with four waving cycles owing to the alternating changes in internal turgor pressure in the sister cells of a dividing Bgs4-depleted cell.** 81X-*bgs4*$^{+}$ cells were grown in the presence of thiamine and 1.2 M sorbitol for 9 h at 30°C and imaged by time-lapse phase-contrast and CW staining (5 µg/ml) microscopy, using an inverted microscope (IX71; Olympus) equipped with a Personal DeltaVision system (Applied Precision). Cells were observed for 180 min. Frames of selected cells were taken every 20 s. To decrease the movie length, the frames only show the stages of septum formation and septum swinging with four waving cycles (t = 166 min).

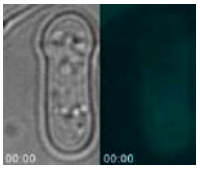

Video 10. **Formation and maturation of a septum followed by cell lysis and release of cytoplasmic material from either one or both sister cells at the start of cell separation of three dividing Bgs4-depleted cells.** 81X-*bgs4*$^{+}$ cells were grown in the presence of thiamine and 1.2 M sorbitol for 10 h at 30°C and imaged by time-lapse phase-contrast and CW staining (5 µg/ml) microscopy, using an inverted microscope (IX71; Olympus) equipped with a Personal DeltaVision system (Applied Precision). Cells were observed for 180 min. Frames of selected cells were taken every 20 s. To decrease the movie length, the frames only show septum formation, cell lysis, and the release of cytoplasmic material from either one (cells 1 and 3) or both sister cells (cell 2) at the start of cell separation (t = 40 and 42 min). Video 9 also shows the cell lysis of both sister cells at the start of cell separation (cell 2), and the cell lysis at the pole of one sister cell (cells 1 and 3) caused by the increased internal pressure generated by the curved septum.

Table S1. **Fission yeast strains used in this study**

Strain	Genotype	Source
33	972 h$^-$	P. Munz[a]
132	*cwg1-1 leu1-32* h$^-$	J. Ribas
296	*cwg1-1 ura4-Δ18* h$^+$	J. Ribas
105	*cwg1-2 leu1-32 ura4-Δ18* h$^+$	J. Ribas
156	*cwg1-2 leu1-32* h$^-$	J. Ribas
419	*leu1-32 ura4-Δ18* h$^-$	J. Ribas
420	*leu1-32 ura4-Δ18* h$^+$	J. Ribas
284	*leu1-32 ura4-Δ18 his3-Δ1* h$^-$	J. Ribas
285	*leu1-32 ura4-Δ18 his3-Δ1* h$^+$	J. Ribas
251	*leu1-32 ura4-Δ18 his3-Δ1 ade6-M210* h$^+$	J. Ribas
252	*leu1-32 ura4-Δ18 his3-Δ1 ade6-M210* h$^-$	J. Ribas
498	*leu1-32 ura4-Δ18 his3-Δ1 bgs4Δ::ura4$^+$* h$^-$ p81XH-*bgs4$^+$*	J. Ribas
1288	*leu1-32 ura4-Δ18 his3-Δ1 bgs4Δ::ura4$^+$* P*nmt1$^+$*-81X-*bgs4$^+$:his3$^+$* h$^-$	This study
1366	*leu1-32 ura4-Δ18 his3-Δ1 ade6-M210 bgs4Δ::ura4$^+$* P*nmt1$^+$*-81X-*bgs4$^+$:his3$^+$* h$^-$	This study
1368	*leu1-32 ura4-Δ18 his3-Δ1 ade6-M210 bgs4Δ::ura4$^+$* P*nmt1$^+$*-81X-*bgs4$^+$:his3$^+$* h$^+$	This study
1493	*leu1-32 ura4-Δ18 his3-Δ1 ade6-M210 bgs4Δ::ura4$^+$* P*nmt1$^+$*-81X-*GFP-bgs4$^+$:his3$^+$* h$^-$	This study
1757	*leu1-32 ura4-Δ18 ade6-M210 GFP-cdc15$^+$:KanMX6* h$^-$	T. Pollard[b]
1777	*leu1-32 ura4-Δ18 his3-Δ1 ade6-M210 GFP-cdc15$^+$:KanMX6* h$^+$	J. Ribas
1756	*leu1-32 ura4-Δ18 rlc1$^+$-GFP:KanMX6* h$^-$	V. Simanis[c]
1793	*leu1-32 ura4-Δ18 his3-Δ1 ade6-M210 rlc1$^+$-GFP:KanMX6* h$^+$	J. Ribas
1522	*leu1-32 ura4-Δ18 his3-Δ1 myo2$^+$-GFP:ura4$^+$* h$^+$	M. Balasubramanian[d]
1520	*leu1-32 ura4-Δ18 ade6-M210 myo3$^+$-GFP:KanMX6* h$^+$	T. Pollard
1873	*leu1-32 ura4-Δ18 GFP-rho2$^+$:KanMX6* h$^+$	P. Pérez
1874	*leu1-32 ura4-Δ18 GFP-rho3$^+$:KanMX6* h$^+$	P. Pérez
1912	*leu1-32 ura4-Δ18 rho4Δ::KanMX6 GFP-rho4$^+$:leu1$^+$* h$^+$	P. Pérez
1949	*leu1-32 ura4-Δ18 rho5Δ::KanMX6 GFP-rho5$^+$:leu1$^+$* h$^+$	P. Pérez
1878	*leu1-32 ura4-Δ18 GFP-cdc42$^+$:KanMX6* p41X-*HA-cdc42$^+$* h$^+$	P. Pérez
2143	*leu1-32 ura4-Δ18 his3-Δ1 rgf1$^+$-GFP:leu1$^+$* h$^+$	Y. Sánchez[e]
2129	*leu1-32 ura4-Δ18 his3-Δ1 rgf3Δ::ura4$^+$ rgf3$^+$-GFP:leu1$^+$* h$^-$	Y. Sánchez
520	*leu1-32 ura4-Δ18 his3-Δ1 bgs1Δ::ura4$^+$* P*bgs1$^+$::GFP-bgs1$^+$:leu1$^+$* h$^+$	J. Ribas
4868	*leu1-32 ura4-Δ18 his3-Δ1 ade6-M? rlc1$^+$-2xRFP:NatMX6* h$^-$	P. Pérez
5016	*leu1-32 GFP-psy1$^+$:leu1$^+$* h^{90}	C. Shimoda[f]
5045	*leu1-32 ura4-Δ18 rlc1$^+$-2xRFP:NatMX6 GFP-psy1$^+$:leu1$^+$* h$^+$	R. Martín-García[e]
1217	*leu1-32 ura4-Δ18 his3-Δ1 bgs3Δ::ura4$^+$* P*bgs3$^+$::GFP-bgs3$^+$:leu1$^+$* h$^+$	J. Ribas
561	*leu1-32 ura4-Δ18 his3-Δ1 bgs4Δ::ura4$^+$* P*bgs4$^+$::GFP-bgs4$^+$:leu1$^+$* h$^-$	J. Ribas
1731	*leu1-32 ura4-Δ18 his3-Δ1 bgs1Δ::ura4$^+$* P*bgs1$^+$::2xGFP-bgs1$^+$:leu1$^+$* h$^+$	This study
1780	*leu1-32 ura4-Δ18 his3-Δ1 bgs1Δ::ura4$^+$* P*bgs1$^+$::2xRFP-bgs1$^+$:leu1$^+$* h$^-$	This study
3166	*leu1-32 ura4-Δ18 his3-Δ1 ade6-M210 ags1Δ* 3′UTR$_{ags1+}$*::ags1$^+$-GFP:leu1$^+$:ura4$^+$* h$^-$	J. Ribas
3169	*leu1-32 ura4-Δ18 his3-Δ1 ags1Δ* 3′UTR$_{ags1+}$*::ags1$^+$-GFP:leu1$^+$:ura4$^+$* h$^+$	J. Ribas
3332	*leu1-32 ura4-Δ18 his3-Δ1 bgs1Δ::ura4$^+$* P*bgs1$^+$::2xRFP-bgs1$^+$:leu1$^+$ bgs3Δ::ura4$^+$* P*bgs3$^+$::GFP-bgs3$^+$:leu1$^+$* h$^-$	This study
3311	*leu1-32 ura4-Δ18 his3-Δ1 rlc1$^+$-GFP:KanMX6 bgs1Δ::ura4$^+$* P*bgs1$^+$::2xRFP-bgs1$^+$:leu1$^+$* h$^-$	This study
2112	*leu1-32 ura4-Δ18 his3-Δ1 ade6-M210 GFP-cdc15$^+$:KanMX6 bgs4Δ::ura4$^+$* P*nmt1$^+$*-81X-*bgs4$^+$:his3$^+$* h$^-$	This study
2209	*leu1-32 ura4-Δ18 his3-Δ1 ade6-M210 rlc1$^+$-GFP:KanMX6 bgs4Δ::ura4$^+$* P*nmt1$^+$*-81X-*bgs4$^+$:his3$^+$* h$^-$	This study
2308	*leu1-32 ura4-Δ18 his3-Δ1 myo2$^+$-GFP:ura4$^+$ bgs4Δ::ura4$^+$* P*nmt1$^+$*-81X-*bgs4$^+$:his3$^+$* h$^-$	This study
2166	*leu1-32 ura4-Δ18 his3-Δ1 ade6-M210 myo3$^+$-GFP:KanMX6 bgs4Δ::ura4$^+$* P*nmt1$^+$*-81X-*bgs4$^+$:his3$^+$* h$^-$	This study
2093	*leu1-32 ura4-Δ18 his3-Δ1 ade6-M210 GFP-rho2$^+$:KanMX6 bgs4Δ::ura4$^+$* P*nmt1$^+$*-81X-*bgs4$^+$:his3$^+$* h$^+$	This study
2095	*leu1-32 ura4-Δ18 his3-Δ1 ade6-M210 GFP-rho3$^+$:KanMX6 bgs4Δ::ura4$^+$* P*nmt1$^+$*-81X-*bgs4$^+$:his3$^+$* h$^-$	This study
2097	*leu1-32 ura4-Δ18 his3-Δ1 ade6-M210 rho4Δ::KanMX6 GFP-rho4$^+$:leu1$^+$ bgs4Δ::ura4$^+$* P*nmt1$^+$*-81X-*bgs4$^+$:his3$^+$* h$^+$	This study
2488	*leu1-32 ura4-Δ18 his3-Δ1 rho5Δ::KanMX6 GFP-rho5$^+$:leu1$^+$ bgs4Δ::ura4$^+$* P*nmt1$^+$*-81X-*bgs4$^+$:his3$^+$* h$^+$	This study
2168	*leu1-32 ura4-Δ18 his3-Δ1 ade6-M210 GFP-cdc42$^+$:KanMX6 bgs4Δ::ura4$^+$* P*nmt1$^+$*-81X-*bgs4$^+$:his3$^+$* h$^-$	This study
2304	*leu1-32 ura4-Δ18 his3-Δ1 rgf1$^+$-GFP:leu1$^+$ bgs4Δ::ura4$^+$* P*nmt1$^+$*-81X-*bgs4$^+$:his3$^+$* h$^-$	This study
2306	*leu1-32 ura4-Δ18 his3-Δ1 rgf3Δ::ura4$^+$ rgf3$^+$-GFP:leu1$^+$ bgs4Δ::ura4$^+$* P*nmt1$^+$*-81X-*bgs4$^+$:his3$^+$* h$^-$	This study
2300	*leu1-32 ura4-Δ18 his3-Δ1 bgs1Δ::ura4$^+$* P*bgs1$^+$::2xGFP-bgs1$^+$:leu1$^+$ bgs4Δ::ura4$^+$* P*nmt1$^+$*-81X-*bgs4$^+$:his3$^+$* h$^+$	This study
2503	*leu1-32 ura4-Δ18 his3-Δ1 ade6-M210 bgs1Δ::ura4$^+$* P*bgs1$^+$::2xRFP-bgs1$^+$:leu1$^+$ bgs4Δ::ura4$^+$* P*nmt1$^+$*-81X-*bgs4$^+$:his3$^+$* h$^-$	This study

Table S1. **Fission yeast strains used in this study** *(Continued)*

Strain	Genotype	Source
1362	*leu1-32 ura4-Δ18 his3-Δ1 bgs3Δ::ura4⁺ Pbgs3⁺::GFP-bgs3⁺:leu1⁺ bgs4Δ::ura4⁺ Pnmt1⁺-81X-bgs4⁺:his3⁺* h⁻	This study
2158	*leu1-32 ura4-Δ18 his3-Δ1 bgs1Δ::ura4⁺ Pbgs1⁺::2xRFP-bgs1⁺:leu1⁺ bgs3Δ::ura4⁺ Pbgs3⁺::GFP-bgs3⁺:leu1⁺ bgs4Δ::ura4⁺ Pnmt1⁺-81X-bgs4⁺:his3⁺* h⁺	This study
3181	*leu1-32 ura4-Δ18 his3-Δ1 ags1Δ* 3′UTR$_{ags1+}$*::ags1⁺-GFP:leu1⁺:ura4⁺ bgs4Δ::ura4⁺ Pnmt1⁺-81X-bgs4⁺:his3⁺* h⁺	This study
5202	*leu1-32 ura4-Δ18 his3-Δ1 rlc1⁺-2xRFP:NatMX6 GFP-psy1⁺:leu1⁺ bgs4Δ::ura4⁺ Pnmt1⁺-81X-bgs4⁺:his3⁺* h⁺	This study
5195	*cwg1-1 leu1-32 ura4-Δ18 rlc1⁺-GFP:KanMX6 bgs1Δ::ura4⁺ Pbgs1⁺::2xRFP-bgs1⁺:leu1⁺* h⁻	This study
5215	*cwg1-2 leu1-32 ura4-Δ18 his3-Δ1 rlc1⁺-GFP:KanMX6 bgs1Δ::ura4⁺ Pbgs1⁺::2xRFP-bgs1⁺:leu1⁺* h⁻	This study
5218	*cwg1-1 leu1-32 ura4-Δ18 rlc1⁺-2xRFP:NatMX6 GFP-psy1⁺:leu1⁺* h⁺	This study
5220	*cwg1-2 leu1-32 ura4-Δ18 rlc1⁺-2xRFP:NatMX6 GFP-psy1⁺:leu1⁺* h⁺	This study

[a]Institute of General Microbiology, University of Bern, Bern, Switzerland.
[b]Department of Molecular, Cellular and Developmental Biology, Yale University, New Haven, CT.
[c]School of Life Sciences, École Polytechnique Fédérale de Lausanne, Lausanne, Switzerland.
[d]Temasek Life Sciences Laboratory and the Department of Biological Sciences, National University of Singapore, Singapore, Singapore.
[e]Instituto de Biología Funcional y Genómica, Consejo Superior de Investigaciones Científicas/Universidad de Salamanca, Salamanca, Spain.
[f]Department of Biology, Graduate School of Science, Osaka City University, Osaka, Japan.